Bone microenvironment regulative hydrogels with ROS scavenging and prolonged oxygen-generating for enhancing bone repair

Han Sun [a,b,c,d], Juan Xu [a,b,c], Yangyufan Wang [a,b,c], Siyu Shen [a,b,c], Xingquan Xu [a,b,c,***], Lei Zhang [a,b,c,**], Qing Jiang [a,b,c,*]

[a] State Key Laboratory of Pharmaceutical Biotechnology, Division of Sports Medicine and Adult Reconstructive Surgery, Department of Orthopedic Surgery, Nanjing Drum Tower Hospital, The Affiliated Hospital of Nanjing University Medical School, 321 Zhongshan Road, Nanjing, 210008, Jiangsu, PR China
[b] Branch of National Clinical Research Center for Orthopedics, Sports Medicine and Rehabilitation, PR China
[c] Co-innovation Center of Neuroregeneration, Nantong University, 9 Seyuan Road, Nantong, 226019, Jiangsu, PR China
[d] Articular Orthopaedics, The Third Affiliated Hospital of Soochow University, 185 Juqian Road, Changzhou, 213003, Jiangsu, PR China

ARTICLE INFO

ABSTRACT

Large bone defects resulting from fractures and disease are a major clinical challenge, being often unable to heal spontaneously by the body's repair mechanisms. Lines of evidence have shown that hypoxia-induced over-production of ROS in bone defect region has a major impact on delaying bone regeneration. However, replenishing excess oxygen in a short time cause high oxygen tension that affect the activity of osteoblast precursor cells. Therefore, reasonably restoring the hypoxic condition of bone microenvironment is essential for facilitating bone repair. Herein, we designed ROS scavenging and responsive prolonged oxygen-generating hydrogels (CPP-L/GelMA) as a "bone microenvironment regulative hydrogel" to reverse the hypoxic microenvironment in bone defects region. CPP-L/GelMA hydrogels comprises an antioxidant enzyme catalase (CAT) and ROS-responsive oxygen-releasing nanoparticles (PFC@PLGA/PPS) co-loaded liposome (CCP-L) and GelMA hydrogels. Under hypoxic condition, CPP-L/GelMA can release CAT for degrading hydrogen peroxide to generate oxygen and be triggered by superfluous ROS to continuously release the oxygen for more than 2 weeks. The prolonged oxygen enriched microenvironment generated by CPP-L/GelMA hydrogel significantly enhanced angiogenesis and osteogenesis while inhibited osteoclastogenesis. Finally, CPP-L/GelMA showed excellent bone regeneration effect in a mice skull defect model through the Nrf2-BMAL1-autophagy pathway. Hence, CPP-L/GelMA, as a bone microenvironment regulative hydrogel for bone tissue respiration, can effectively scavenge ROS and provide prolonged oxygen supply according to the demand in bone defect region, possessing of great clinical therapeutic potential.

1. Introduction

Critical-sized bone defects, caused by trauma, infection, tumor resection, and bone abnormalities in orthopedic surgery, cannot heal spontaneously within a patient's lifetime. Although bone grafts have widely been used in the clinic to augment bone regeneration and repair, bone tissue engineering (BTE) holds the promise in the treatment of large bone defects due to advancement of novel biomaterial with facile fabrication and wide accessibility [1]. Tissue regeneration is a dynamic process involving a bidirectional interplay between cells and their surrounding matrix, and this dynamic reciprocity is encouraged by biomaterial designs that are adaptive to local cellular changes and can alter their properties in response to local biological signals. Additionally, bone defects are often accompanied by local microvascular ruptures, and the bone regeneration in the hypoxic microenvironment caused by the interruption of blood supply is still a challenge [2,3]. It is well-known that low-oxygen level can not only affect the proliferation and viability of bone marrow mesenchymal stem cells (BMSC) *in vitro*, but also inhibit the metabolic transformation and osteogenesis of BMSC, which in turn significantly reduce the expression of osteogenic markers and mineralization [4,5]. Study of Huang et al. showed that 2% oxygen reduction can affect mineralization and alkaline phosphatase (ALP) activity during osteogenesis [6]. Therefore, hypoxia will reduce the therapeutic effect of bone regeneration and repair. In addition to directly reducing cell activity, hypoxia is also conducive to the increase of pro-inflammatory mediators such as reactive oxygen species (ROS) [7]. High concentration of ROS can induce cell death in osteoblast precursor cells and mature osteoblasts, and can interfere with the osteogenic differentiation of BMSC and osteoblast precursor MC3T3-E1 cells by inhibiting the expression of osteogenic markers of ALP, osteocalcin (OCN) and runt-related transcription factor 2 (RUNX2) [8–10]. On the contrary, ROS can trigger the oxidation of tyrosine kinase and protein tyrosine phosphatase 1 to regulate Akt and ERK, so as to improve the proliferation and activity of osteoclast progenitor cells, and finally affect the regulation of bone homeostasis [11,12]. Therefore, reasonable oxygen supply and ROS scavenging are of great significance to promote the regeneration of bone tissue.

However, current treatment strategy for overcoming hypoxic conditions within a tissue engineering scaffold is to increase the level of oxygen within the scaffold by using perfluorocarbons (PFCs) [13–15]. Based on the outstanding characteristics of PFC, these systems possess high oxygen carrying capacity with good biosafety. However, the oxygen release rate of these PFC based systems is mostly very fast, which lasts only a few days or even hours. More importantly, hypoxia caused redox imbalance, like ROS overproduction, almost not be taken into consideration in these studies. Therefore, some other studies focus on ROS and apply components such as manganese dioxide or catalase to convert ROS into oxygen [7,16–19]. These materials show excellent ROS scavenging capacity, but they do not contain additional oxygen reserves, and the amount of released oxygen is highly dependent on the concentration of ROS. Moreover, current oxygen-releasing scaffolds can hardly change the release rate and provide prolonged oxygen supply according to the demand in defect region. Therefore, smart BTE materials for regulating oxygen microenvironment that holds the great promising for promoting bone regeneration in clinic are still expected.

Hyperbaric oxygenation therapy, which elevates oxygen levels in tissues, was found to increase osteoblast activity and accelerate bone formation. However, if a large amount of oxygen is supplied blindly in a short time, it is easy to cause high oxygen tension and reduce the proliferation ability of osteoblast precursor cells [20]. Therefore, it is necessary to build an intelligent sustained-release system to achieve the controllable release of O2. Poly (propylene sulphide) (PPS) is a hydrophobic block in the conventional state. Interestingly, after triggering by ROS, the sulphide in the central region of PPS can partially oxidized to sulphoxides and finally oxidized to sulphones, so as to increase the hydrophilicity of the initial hydrophobic central region, which drives

micelle decomposition and lead to drug release [21]. This process only occurs in pathological sites where the concentration of ROS is much higher than that of normal tissues [22], which gives the potential to achieve the controllable release of oxygen at the hypoxia site of bone defect. In terms of oxygen carrying materials, the van der Waals' force between PFC molecules is very weak, so that liquid PFC can dissolve a large amount of O2 and transport it to anoxic tissues through passive diffusion [23]. Unlike the directional chemical binding in hemoglobin, the gas dissolution in PFC follows Henry's Law (i.e. proportional to the partial pressure of the gas) [24]. Therefore, hypoxic tissue can quickly and massively extract oxygen from PFC [25–27]. More importantly, PFC related products have achieved remarkable results in the phase III clinical trials of islet hypoxia protection and surgical blood transfusion [26,28,29]. Despite smart oxygen production could relief hypoxia, the hypoxia induced ROS could also affects osteoclastogenesis, which can induce bone reabsorption, inhibit bone formation, and even cause osteoporosis. Catalase (CAT) is an important member of antioxidant enzyme system, the function of which is to promote the decomposition of H2O2 into O2 and H2O, so as to protect the function of antioxidant enzyme system to prevent the invasion of H2O2 to cells [30,31]. It is also of great significance for human growth, development, and metabolic activities. Hence, the combination of CAT and PFC could efficiently regulate the vicious cycle of hypoxia-ROS, and recovering the microenvironment of bone defect by oxygen therapy. Therefore, we integrate these aspects together, and a new material is expected to be developed to meet the requirements.

At present, the commonly used oxygen-generating materials possess fast oxygen release rate so that are commonly used for wound treatment [32–34]. More importantly, these materials can hardly accelerate the oxygen supply rate according to the degree of hypoxia in the damaged area. Herein, we employed a composite hydrogel material with the potential of ROS-scavenging and prolonged oxygen supply according to the demand in bone defect region (Fig. 1). The novel composite hydrogel material could convert ROS into O2 and further response to the superfluous ROS, which was caused by the uncorrected hypoxia, to accelerate O2 generation according to the demand in defect region. The oxygen loaded PFC was encapsulated in PLGA/PPS nanoparticles to construct the oxygen loaded nanoparticles with intelligent release property. Subsequently, PFC@PLGA/PPS nanoparticles combined with CAT were loaded in liposomes (Lip), and finally encapsulated with GelMA hydrogel to construct the novel material of CPP-L/GelMA. The abilities of the CPP-L/GelMA hydrogel in scavenging ROS and generating O2 were investigated *in vitro*. Then, we examined the effect of the CPP-L/GelMA hydrogel on promoting vascular ring formation, inhibiting osteoclast differentiation, and promoting osteoblast differentiation under hypoxia condition. The possible mechanism during osteogenesis was also explored concurrently. Finally, a mice skull defect model was used to detect the ability of the CPP-L/GelMA hydrogel in promoting bone regeneration. By closely following the challenge of hypoxic microenvironment in bone defect area and skillfully utilizing the relationship between hypoxia and ROS production, this study innovatively constructs an ROS-scavenging and O2 intelligent prolonged release hydrogel, which is expected to construct a new concept of BTE material and provide an effective and intelligent strategy for bone defect repair.

2. Materials and methods

2.1. Materials

Polyvinyl alcohol (PVA) was purchased from Beijing Solarbio Science & Technology Co. Ltd. (China). was Soy phosphatidylcholine (SPC) and cholesterol were purchased from Aladdin Industrial Corporation (China), and DSPE-PEG2000 was obtained from A.V.T. Pharm. Ltd. (China). Anaeropack was from Mitsubishi Gas Chemicals (Japan). Poly (D, L-lactide-co-glycolide) (PLGA) (lactide: glycolide = 50 : 50, MW = 7000) and Tartrate-resistant acid phosphatase (TRAP) staining kits were

purchased from Sigma-Aldrich (USA). Perfluoro-15-crown-5-ether (PFC, 99%, MW = 580.08) was obtained from J&K Scientific Ltd.. All chemicals used in this work were of analytical grade and were used as received. Catalase Assay Kit was from KeyGen Biotec Co. Ltd. (China). Cell culture mediums and fetal bovine serum were purchased from Wisent Corporation (China). Transwell (0.4 μm) was from Corning (USA). Macrophage colony-stimulating factor (M-CSF) and receptor activator of nuclear factor-kappa B ligand (RANKL) were purchased from R&D (USA). The 2′,7′-Dichlorodihydrofluorescein diacetate (H2DCFDA) was purchased from MedChemExpress (USA). Phalloidin was from ThermoFisher Scientific (USA). The CellTiter 96® AQueous One Solution Cell Proliferation Assay (MTS) was purchased from Promega (USA). OriCell® mouse MC3T3-E1 cells osteogenic differentiation kit and rlizarin red staining (ARS) kit were from Cyagen (China). ALP staining kits and 3,3′-diaminobenzidine (DAB) horseradish peroxidase color development kits were purchased from Beyotime (China). Lipofectamine 3000 was from Thermo Fisher (USA). Type I collagen (Col I), osteopontin (OPN), brain and muscle arnt-like Protein 1 (BMAL1), nuclear factor (erythroid-derived) 2)-like 2 (NRF2), Beclin1, microtubule-associated proteins light chain 3 (LC3), CD31, β-actin primary antibodies, peroxidase-conjugated secondary antibodies, fluorescent secondary antibodies, and HRP-conjugated secondary antibody were purchased from Proteintech (USA). RUNX2 primary antibody was from Cell Signaling Technology (USA). Fetal liver kinase-1 (Flk-1) primary antibody was purchased from Abcam (USA). Hypersensitive enhanced chemiluminescent chemiluminescence kit was from New Cell & Molecular Biotech Co., Ltd (China). Bovine serum albumin (BSA) was purchased from Biosharp (China). Goat serum (10%) was from Boster (China). The 4′,6-diamidino-2-phenylindole (DAPI) was purchased from KeyGEN Bio TECH (China). ROS Brite™ 700 was from AAT Bioquest

(USA). Hypoxyprobe™-1 Plus Kit was purchased from Chemicon International (USA).

2.2. Fabrication and characterization of CPP-L/GelMA

2.2.1. PFC@PLGA/PPS nanoparticles synthesis

The PFC loaded nanoparticles were prepared using a double emulsion (water/oil/water) solvent evaporation process [13,14]. Briefly, PFC solution (20 μL) was added to PLGA/PPS (2.4 mg, W/W = 1:1) dissolved in dichloromethane (100 μL), into which 5% PVA solution (w/v) (1 mL) was then added. The mixture was sonicated using a sonifier equipped with microtip in an ice water bath for 5 min. Then another 0.6 mL PVA solution was added to homogenize the emulsion. The product was then centrifuged at 14800 rpm for 10 min at 4 °C, and washed several times with purified water to remove PVA. The final product of PFC@PLGA/PPS nanoparticles were collected and stored in deionized water at 4 °C for future use.

2.2.2. CAT-PFC@PLGA/PPS@Lip nanoparticles (CPP-L) synthesis

CAT loaded liposomes were prepared using the film dispersion method [35]. CAT loaded liposomes containing SPC, cholesterol, and 1, 2-distearoyl-sn-glycero-3-phosphoethanolamine 2000 (DSPE-PEG 2000) were dissolved in 1 mL of chloroform at a molar ratio of 10:1:3. They were then dried under vacuum to remove residual chloroform and obtain a thin lipid film. The thin lipid films were dispersed in 2 mL of phosphate-buffered saline (PBS) containing 3 mg CAT for hydration. CAT-Liposomes were prepared after filtration through 200 nm polycarbonate membrane filters (Millipore, Billerica, USA). Next, 0.6 mL PFC@PLGA/PPS was incubated with 1 mL CAT-Liposome at 4 °C overnight. After centrifuged, CAT-PFC@PLGA/PPS@Lip (CPP-L) was
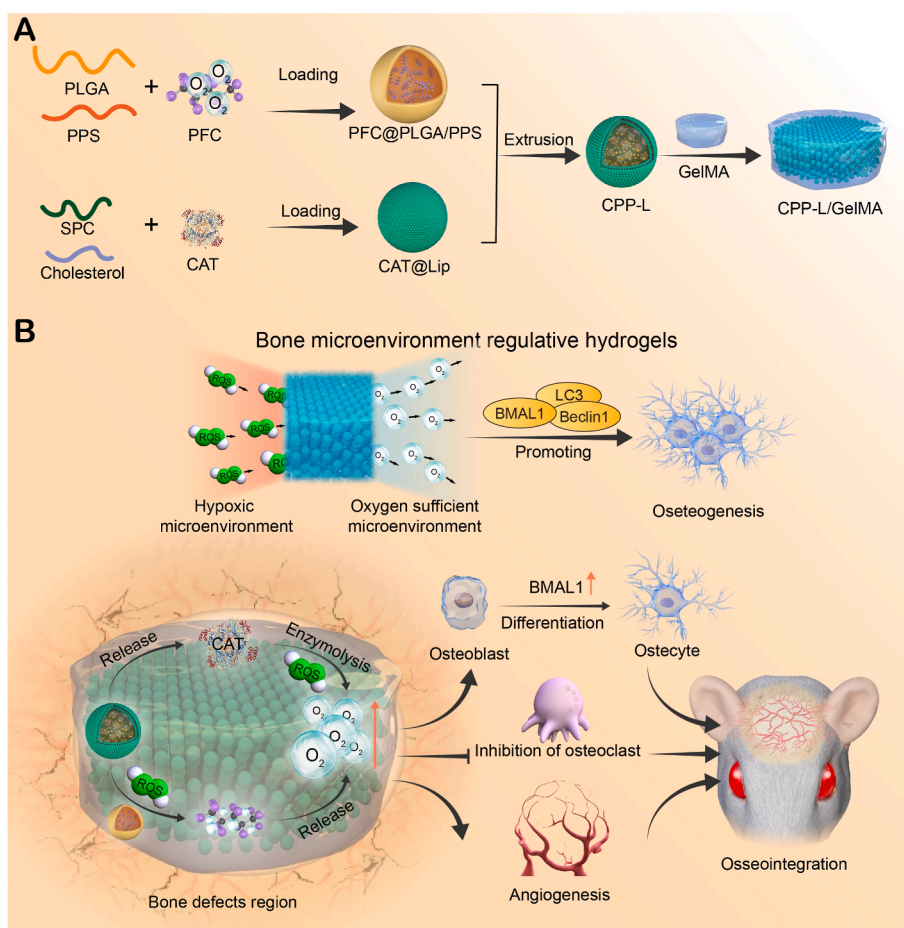
Fig. 1. Schematic illustration of bone microenvironment regulative hydrogels with ROS scavenging and prolonged oxygen-generating for enhancing bone repair. (A) The PFC loaded in PLGA/PPS nanoparticles to form PFC@PLGA/PPS nanoparticles. Liposomes was used to co-load PFC@PLGA/PPS nanoparticles and CAT to construct CPP-L, which further encapsulated in a GelMA hydrogel and finally build up the CPP-L/GelMA intelligent response oxygen-releasing hydrogel. (B) The CPP-L/GelMA can act as a "bone microenvironment regulative hydrogel" to reverse the hypoxic microenvironment in bone defects region to promote osteogenesis. In detail, after implanted into the bone defect site with CPP-L/GelMA, the release of CAT can generate oxygen by the enzymatic hydrolysis of ROS caused by the hypoxic microenvironment. Moreover, the superfluous ROS triggers PFC@PLGA/PPS nanoparticles to release oxygen which then burst the liposome and disperse into the surrounding environment for a further oxygen supply. ROS scavenging and oxygen production promote osteoblast differentiation through the BMAL1-autophagy pathway and inhibit osteoclast formation, as well as promote neovascularization, which finally accelerate bone regeneration.

obtained after strained 50 times through a 100 nm filter at 4 °C.

Then we measured the oxygen carrying ability of CPP-L nanoparticles following pervious report [13]. Firstly, 200 μL of CPP-L solution stored in a 15 mL sample tube was diluted to 2 mL with deionized water, and then placed in an aseptic oxygen chamber (O2 flow rate = 5 L/min) for 20 s for oxygenation. Afterwards, the oxygen concentrations in aqueous solutions (4 mL) were measured with an oxygen probe (OX-NP, Unisense A/S CO.LTD) [15] before and after adding 2 mL CPP-L solution. In addition, CPP-L solution without oxygenation, PFC@PLGA/PPS solution with oxygenation, H_2O with oxygenation, and H_2O without oxygenation were used as control groups.

2.2.3. Preparation of composite hydrogels

CPP-L/GelMA composite hydrogels were fabricated by adding CPP-L into 5% w/v GelMA solution with 0.25% w/v photoinitiator lithium phenyl-2,4,6-trimethylbenzoylphosphinate (LAP), then irradiated with a UV light source flashlight (with a wavelength of 405 nm) for 1 min. A 5% GelMA hydrogel was used as control group.

2.2.4. Mechanical tests

To test the mechanical property of composite hydrogels, cylindrical samples of the hydrogels (diameter, 4.5 mm; height, 5 mm) were fabricated, and subsequently subjected to a Young's modulus test which was calculated as the slope of the linear region in the stress-strain curve obtained by an universal mechanical testing system (68SC, Instron, Boston, USA) [36,37].

2.2.5. Degradability of CPP-L/GelMA

CPP-L/GelMA were suspended in neutral (pH 7.4) phosphate buffer solutions. Samples were incubated in a shaker at 37 °C. The lost weight was measured after freeze drying at 0, 0.2, 0.3, 0.5, 1, 2, 3, 6, 8, 12, 14, 16, 18, 20, 22, 24 days.

2.2.6. Morphology of nanoparticles, hydrogels, and composite hydrogels (CPP-L/GelMA)

The morphology of nanoparticles (PFC@PLGA/PPS and CPP-L) was examined using a transmission electron microscopy (TECNAI G2 F20, FEI, USA) at an accelerating voltage of 30 kV. The GelMA hydrogels and CPP-L/GelMA composite hydrogels were dried using a freeze dryer. Platinum was sprayed at 20 mA for 45 s, and the cross-sectional morphology of the samples was observed using a scanning electron microscopy (SEM: Quanta 250, FEI, Hillsboro, OR, USA).

2.2.7. In vitro release property assay

In vitro release study was performed in PBS (0.1 M, pH 7.4) solution containing H_2O_2 at a concentration of 10 mM at 37 °C [38]. Typically, CPP-L/GelMA (2 mg) was dispersed into PBS at 37 °C. The solutions were centrifuged to collect the supernatants at different time points (0, 1, 2, 4, 8, 10, 12, and 14 d). The CAT in the supernatant was determined with Catalase Assay Kit.

2.2.8. Measurement of O_2 production

A portable dissolved oxygen meter was utilized to detect the O_2 concentrations in aqueous solutions. After co-incubated with H_2O_2 (10 mM), the catalytic ability of CPP-L/GelMA hydrogel (containing 100 μL CPP-L and 5% Gelma hygrogel) was evaluated at different times, CPP-L and PFC@PLGA/PPS was taken as control. Then an oxygen probe (OX-NP, Unisense A/S CO.LTD) [15] was inserted to measure the O_2 concentration of the solution in real time.

2.3. In vitro performance

2.3.1. Cell culture

Cell culture medium contains cell basal medium (88%), fetal bovine serum (10%), and penicillin-streptomycin (1%). Cells were cultured in an incubator at 37 °C and 5% CO_2 with 95% relative humidity. Culture

media was changed every three days. When reaching 80% confluence, MC3T3-E1 cells, RAW264.7 cells, and human umbilical vein endothelial cells (HUVEC) were trypsinized to passage. In the subsequent experiment of co-culture with materials, the cells were placed in the bottom chamber of a 0.4 μm Transwell, while the materials were placed in the upper chamber.

2.3.2. Intracellular ROS measurement

The MC3T3-E1 cells with GelMA hydrogel, CPP-L nanoparticles, or CPP-L/GelMA hydrogel were cultured under a hypoxic condition by using an Anaeropack anaerobic system previously described in other studies. Briefly, the Anaeropack system could absorb oxygen and produces carbon dioxide through the sodium ascorbate, and currently absorb excess carbon dioxide through a carbon dioxide scavenger. Through these components, the oxygen concentration in the Anaeropack anaerobic system could decrease to less than 1% within 1 h and the carbon dioxide concentration maintained around 5% [39–41]. After 12 h of hypoxic culture, cells were incubated with 5 μM of H2DCFDA at 37 °C for 30 min, and then washed with PBS. Intracellular ROS level was measured by a fluorescence microscope (ECLIPSE Ti2; Nikon, Tokyo, Japan). All images were captured under the same conditions, and the fluorescence was quantified by ImageJ software (National Institutes of Health, Bethesda, MD, USA).

2.3.3. In vitro cell proliferation assay

Cell proliferation was observed by Phalloidin/DAPI staining and MTS assay. In brief, after being cultured in hypoxic environment with the Anaeropack anaerobic system for 5 days, cells of each group were fixed with 4% paraformaldehyde (PFA) for 30 min and then blocked with 1% bovine serum albumin (BSA) overnight. Then the cells were washed with PBS and incubated with Phalloidin solution (6.6 μM, 100% methanol) for 30 min at room temperature avoiding light. Finally, the samples were incubated with ready-to-use DAPI staining solution for 5 min at room temperature. The morphology and number of cells were observed under a fluorescence microscope (ECLIPSE Ti2; Nikon, Tokyo, Japan). Subsequently, the quantitative analysis was performed by the MTS assay. The MTS solution and culture medium were added to the 96-well plate (120 μL per well) with a rate of 1:5. After 2 h of culture in the cell incubator, 100 μL of the reacted medium was aspirated from each well to a new 96-well plate. The absorbance value at 490 nm wavelength was read by microplate reader (MK3; ThermoFisher Scientific, Waltham, USA).

2.3.4. In vitro angiogenesis characterization

In order to detect the effect of oxygen release on HUVECs migration under hypoxic microenvironment by using the Anaeropack anaerobic system, the Transwell test was used. HUVECs were implanted into the upper chamber of Transwell at a concentration of 5×10^4 cells per hole. Then the GelMA hydrogel, CPP-L nanoparticles, and CPP-L/GelMA hydrogels were added to the lower layer of a 24-well plate. Then the plate was into an Anaeropack anaerobic system. The next day, the chamber was fixed with 4% paraformaldehyde and then stained by the crystal violet solution. The cells on the upper surface of the membrane were gently wiped with a cotton swab, and the cells on the lower surface of the membrane were observed with a microscope.

To detect the formation of tubes, 200 μL of HUVECs were seeded into 48-well plate at a concentration of 3×10^4 cells/mL with material of each group (no material control group, GelMA group, CPP-L group, and CPP-L/GelMA group). The plate was pre-laied with 4 °C Matrigel. Then the plate was incubated at an anaerobic bag system to form tubes. After 12 h of culture, HUVECs were photographed by microscope to count the number of tubes.

2.3.5. In vitro osteoclast differentiation and characterization

RAW264.7 cells were cultured in high glucose DMEM containing 10% fetal bovine serum and 1% penicillin-streptomycin for 3 days. Then

the adherent cells were cultured with M-CSF (50 ng/mL) and RANKL (100 ng/mL) for 3 days in a hypoxic environment by using the Anaeropack anaerobic system. Cultured cells were fixed with 4% paraformaldehyde and stained by a TRAP kit. Osteoclasts were defined as TRAP-positive cells with more than three nuclei under a microscope.

2.3.6. In vitro osteoblast assay

The MC3T3-E1 cells were seeded on the bottom of each well, and the materials were immersed in the upper chamber. Then the plate was incubated at an Anaeropack anaerobic system. When the cell fusion degree reached 70%, the OriCell® mouse MC3T3-E1 cells osteogenic differentiation kit was used. The differentiation medium was exchanged every three days.

(1) ALP staining

After 7 days of co-culture and induction, the cells were fixed by 4% PFA for 30 min. Then the ALP activity was detected by the ALP staining through an ALP staining kit. After incubating MC3T3-E1 with ALP chromogenic agent for 30 min from the light, the microscope was used to observe the result.

(2) Alizarin red staining

The calcium nodules generated by the cells were stained by an ARS kit. After 21 days of co-culture, the cells were washed with PBS and fixed with 4% PFA for 30 min, followed by the ARS staining for 15 min. The calcium nodules were observed by the camera and microscope. Then, the ARS was dissolved by the alkyl hexadecpyridine solution and the OD values at 562 nm were measured with a microplate reader (MK3; ThermoFisher Scientific, Waltham, USA).

2.3.7. Study on the mechanism of materials promoting osteogenic differentiation

(1) Short interfering RNA (siRNA) transfection

To explore the role of BMAL1 in material promoting osteogenic differentiation, a short interfering RNA (siRNA) against the mice BMAL1 gene (sequence: 5′-CCACAGCACAGGCUAUUUGAATT-3'/5′-UUCAAAUAGCCUGUGCUGUGGTT-3′) was designed and synthesized. Before transfection, the MC3T3-E1 cells were seeded in 6-well plates. After reaching to about 70% confluence, the cells were transfected with 50 nM siRNA^{BMAL1} or negative control loaded in Lipofectamine 3000 for 12 h according to the manufacturer's instruction. Then the cells with or without transfection were all continued to be co-cultured with each kind of materials in an Anaeropack anaerobic system and underwent the osteogenic differentiation.

(2) Western blot analysis

After 10 days of induction, the proteins of cells in each group were extracted by a whole protein extraction kit according to the instruction and then centrifuged for 10 min at 12,000 g at 4 °C. Then the proteins were separated by sodium dodecyl sulfate-polyacrylamide gel electrophoresis using 4–20% gels and transferred to nitrocellulose membranes. The membranes were blocked for 1 h and then incubated with primary antibodies (Col I, OPN, BMAL1, NRF2, Beclin1, LC3, and β-actin) overnight at 4 °C. The membranes were subsequently washed by PBS with 0.1% Tween 20 (PBST) for six times in 30 min. After further incubated with peroxidase-conjugated secondary antibodies for 1 h, immunoreactive bands were detected with a hypersensitive enhanced chemiluminescent chemiluminescence kit.

(3) Immunofluorescence staining

Cells were fixed with 4% PFA for 30 min and then permeabilized with 0.2% Triton-100 in PBS for 20 min. Then, the BSA (5% w/v) was used for blocking at room temperature for 1 h. After the blocking, cells were incubated with primary antibody against BMAL1 or RUNX2 at 4 °C overnight and further stained with secondary antibody with green or red fluorescence respectively at room temperature for 1 h. Finally, DAPI was used to stain the nuclei. The results were observed under a fluorescence microscope (ECLIPSE Ti2; Nikon, Tokyo, Japan).

2.4. In vivo study

All procedures followed the Chinese national guidelines for the care and use of laboratory animals. C57BL/6 wild type mice aged 8 weeks were obtained from the Model Animal Research Center of Nanjing University. Before and after operation, they were maintained in a specific pathogen-free (SPF) environment with freely available water and standard mouse chow. All surgical procedures and perioperative handling were conducted in accordance with protocols approved by the Ethics Committee of the Drum Tower Hospital, Medical School of Nanjing University.

2.4.1. Mice skull defect model and implantation of materials

Before surgery, mice were fed for 1 week in separate cages to adapt to the environment. Anesthesia was performed by inhalation of isoflurane. After incising the skin on the top of head, a circular full thickness bone defect with a diameter of 2.5 mm was created by a drill. Then the defect areas of mice in different groups were filled with different kinds of materials, and the wounds were sutured layer by layer. For the first 3 consecutive days postoperatively, an intramuscular injection of penicillin along with iodine disinfection on the incisions was performed.

2.4.2. Detection of in vivo ROS expression in skull defect area

All the mice skull defect model at 1, 2, 4 or 6 weeks after surgery were probed with ROS Brite™ 700 [42]. Bioluminescence images were recorded to assess the production of ROS in skull defect area. To acquire the *in vivo* bioluminescence signal, mice were firstly anesthetized with isoflurane and ROS Brite™ 700 (*in vivo* imaging solutions, 100 μM in Hanks with 20 mM HHBS) were injected with into the cranial region. Bioluminescence images were acquired using an *in vivo* imaging system (PerkinElmer, Boston, USA).

2.4.3. Labeling of in vivo hypxic cells in skull defect area

In vivo hypoxic cells were labeled by the Hypoxyprobe™-1 Plus Kit according to the instructions [43,44]. In brief, mice were injected with the Hypoxyprobe (pimonidazole hydrochloride) hypoxia marker at a dose of 100 mg/kg into the cranial region at 4 weeks after surgery and euthanized 1 h after injection. Skull tissues were then snap frozen and processed for histology. After incubation with fluorescein isothiocyanate-labeled Hypoxyprobe™-1 monoclonal antibody 1 (mAb1, 1:100 dilution) for 30 min, anti-fluorescein isothiocyanate monoclonal antibody conjugated to horseradish peroxidase provided by the kit was used as a secondary antibody. Finally, the nuclei were stained with DAPI, and a laser confocal microscopy (FV3000; Olympus, Tokyo, Japan) was used for the observation.

2.4.4. Detection of residual oxygen in the CPP-L/GelMA in vivo

At 0 day, 7 days, and 14 days after implanting the CPP-L/GelMA hydrogel in mouse skull defect model, the contents of the bone defect area were taken out and immersed in H_2O_2 solution to promote the release of residual oxygen. Then the oxygen probe (OX-NP, Unisense A/S CO.LTD) [15] was used to detect the concentration of the residual oxygen.

2.4.5. Analysis of microcomputed tomography

Mice were euthanatized at 4 and 8 weeks postoperatively, and the skull specimens were harvested. The specimens were fixed with 10%

formalin, and then scanned by the microcomputed tomography (micro-CT, SkyScan 1176; Bruker, Kontich, Belgium) to evaluate the regenerative condition of the defect areas. The mimic software was used to reconstruct the three-dimensional (3D) structures of the calvarium, and the bone volume/tissue volume (BV/TV) and bone mineral density (BMD) were also calculated.

2.4.6. Histological assessment

The specimens were decalcified with 0.5 M ethylenediaminetetraacetic acid (EDTA) for 2 weeks at room temperature. After embedding in paraffin blocks, the samples were sectioned at a thickness of 5 μm and stained with hematoxylin and eosin (H&E) for histological assessment. A bright field microscope (Zeiss Axiovert 200; Carl Zeiss Inc., New York, USA) was used to capture the images.

2.4.7. Immunohistochemistry staining

The antigen retrieval was first performed on the slices. Then the specimens were incubated with primary antibody against CD31, NRF2, Col I, BMAL1, and LC3 at 4 °C overnight. The next day, HRP-conjugated secondary antibody was added, and the samples were processed with a DAB horseradish peroxidase color development kit and counterstained with hematoxylin. In the CD31 Immunohistochemistry staining assay, the number of blood vessels in each field was also quantitatively analyzed to present the blood vessel density following previously reported methods [45].

2.4.8. Immunofluorescence staining

Immunofluorescence staining of slices was similar to that of cells described previously. Briefly, after antigen retrieval, the slices were blocked with 10% goat serum for 1 h and then incubated with primary antibodies (flk-1, BMAL1, beclin1, and OPN) at 4 °C overnight. The next day, the slices were washed by PBST and then incubated with anti-rabbit fluorescein-conjugated antibody at room temperature for 1 h, followed by nuclei staining with DAPI. A fluorescence microscope was used for capturing the images.

2.5. Statistical analysis

The data analyzed with normalization are specified in the figure legends. All data are presented as the mean $\pm$ SD. For *in vivo* imaging studies, n = 6 mice in each group; otherwise, n = 3 (e.g. BV/TV, Tb. Th, Tb. N, Relative gray value). An unpaired two-tailed *t*-test was used to calculate the significance of differences (*p* value). $p < 0.05$ was considered to demonstrate statistically significant differences. Statistical analysis was performed using SPSS software (version 13.0; Social Inc. IL, Chicago, USA).

3. Results and discussion

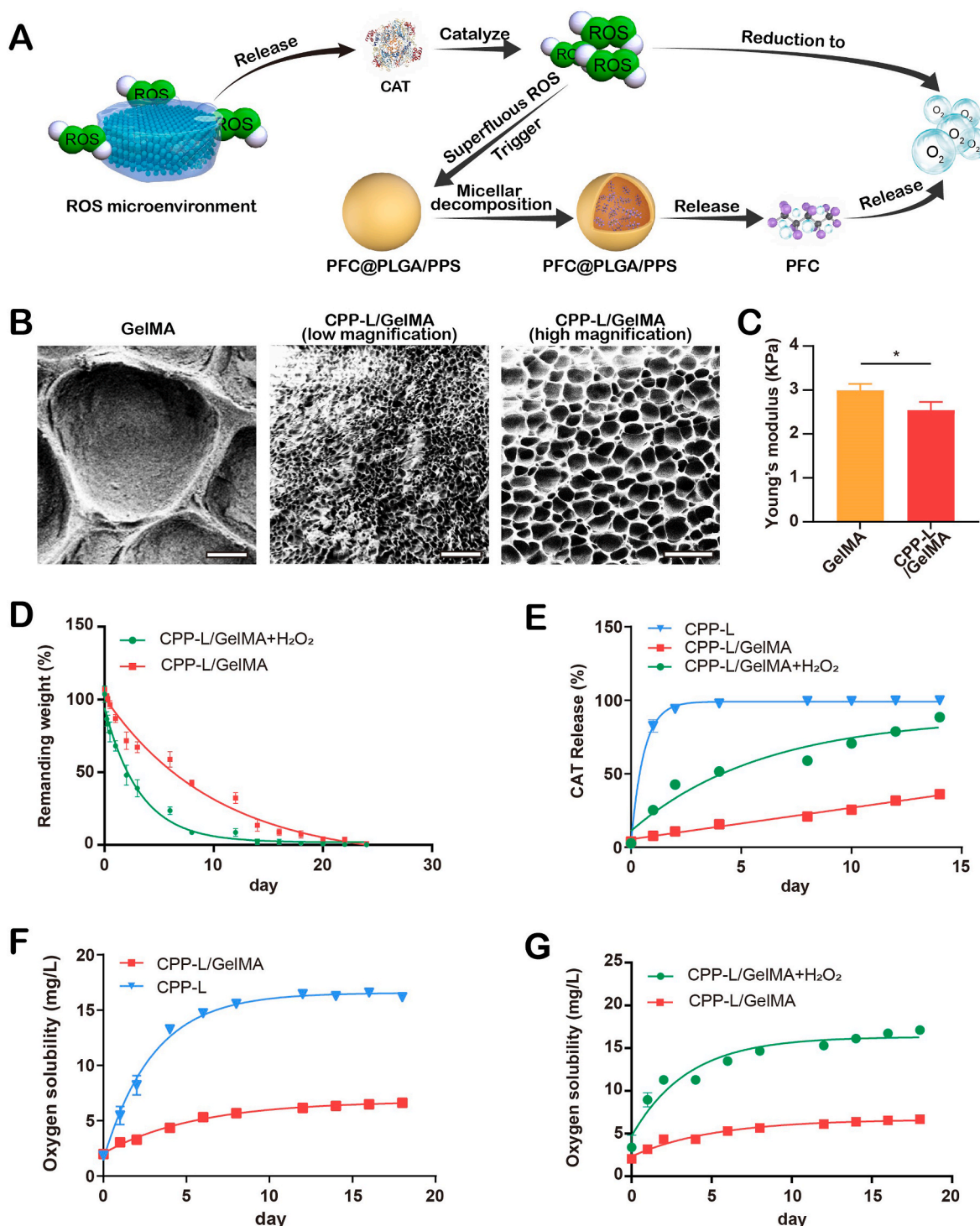### 3.1. Characterizations of CPP-L and composite hydrogels

PFC@PLGA/PPS nanoparticles, which serviced as the ROS triggered oxygen-regenerative nanoparticles, were prepared using a double emulsion (water/oil/water) solvent evaporation process [46]. As shown in Figs. S1 and S2, PFC@PLGA/PPS particles possessed of a core-shell structure with about 40 nm, with a negative Zeta potential about −20 mV (Fig. S3). In addition, CAT, one of the most important antioxidant enzymes, can decompose two hydrogen peroxide molecules into one oxygen molecule and two water molecules through a two-step reaction, making it an effective ROS scavenger and oxygen generator [30,47]. However, the stability of CAT is so poor that it can be quickly scavenged *in vivo*, while being encapsulated in liposomes can effectively improve the stability of CAT [48,49]. Liposomes are a closed phospholipid bilayer vesicle system, which can encapsulate hydrophilic and hydrophobic drugs. Owning to their excellent biocompatibility and biodegradability, liposomes are attractive in the field of drug delivery [50]. In

this study, after co-loaded PFC@PLGA/PPS and CAT into liposomes by using avanti Mini-Extruder, CPP-L were obtained. The CPP-L were spherical and uniform with diameters about 100 nm (Figs. S4 and S5). Moreover, after liposome encapsulation, the CPP-L still revealed a negative Zeta potential (Fig. S6), indicating its good biosafety. Lines of evidence have proven that PFC has high oxygen carrying ability when they flow through blood vessels, we further evaluated the amount of dissolving oxygen inside the PFC core of CPP-L/GelMA hydrogel by using an oxygen probe. After preoxygenated in an aseptic oxygen chamber, the oxygen concentration in PFC@PLGA/PPS were about 10 mg/L, which is nearly the same as CPP-L (Fig. S7), indicating that the additional loading of CAT did not affect the oxygen carrying ability of PFC in CPP-L.

GelMA is a photosensitive hydrogel with biocompatibility and biodegradability, which has been widely used in tissue engineering applications [51]. The high-water content of GelMA hydrogel provides a tissue-like and biocompatible 3D environment for the culture of bone related cells, and its internal relaxed environment is conducive to the formation of bone tissue [52]. In order to further enhance the osteoconductivity, we introduced the GelMA hydrogel to finally form the CPP-L/GelMA by adding CPP-L into GelMA solution to obtain composite hydrogels. Pore size in the composite hydrogels increased with the loading of CPP-L (Fig. 2B). The pores in CPP-L/GelMA allowed for effective oxygen, nutrient, and waste diffusion in a 3D environment, and cell motility, which hold great potential for facilitating bone generation. In addition, the mechanical test results show the Young's modulus of composite hydrogels is relatively decreased (15.14%) with CPP-L content (Fig. 2C). Furthermore, the degradability of CPP-L/GelMA was also evaluated. As shown in Fig. 2D, the degradation period of CPP-L/GelMA hydrogel in neutral solution was as long as 24 days, exhibiting its promising biodegradability *in vitro*. More importantly, after the addition of H_2O_2 the weight of CPP-L/GelMA decreased significantly after 1 day, while CPP-L/GelMA completely decomposed after 12 days. The degradation of CPP-L/GelMA hydrogel in ROS environment suggested that CPP-L/GelMA hydrogel possessed of the durative release of internal functional components (CAT and CPP-L) under hypoxic microenvironment, which could be used for purifying the hypoxic microenvironment of bone defect region [53].

Burst release of growth factors or drugs is easy to cause poisoning or waste due to high local concentration, or be quickly eliminated due to lake of protection [54,55]. Many studies have showed that the addition of GelMA in systems of microcarriers or nanocarriers can provide long-term release of growth factors, GelMA therefore can be used for local factor or drug delivery with excellent bioavailability *in vivo* [56]. As shown in Fig. 2E, compared to CPP-L, the release of CAT from CPP-L/GelMA were obviously slowdown, which is only 36% under physiological condition (pH 7.4) within 15 days, indicating that GelMA can effectively prolonged the release of CAT. Meanwhile, as to the release characteristics of oxygen in our study, it could be found that the release rate of oxygen from CCP-L was significantly decreased after loading in GelMA (Fig. 2F). The oxygen release of CPP-L group gradually entered the plateau stage at 10 days, while the oxygen release in CPP-L/GelMA group still showed low concentration and continuous delivery at 2 weeks, indicating that the oxygen release rate was significantly slowed down with the help of GelMA hydrogel.

Hypoxia is one of the main reasons for reducing the therapeutic effect of bone regeneration. In addition, hypoxia is conducive to the increase of pro-inflammatory mediators such as reactive oxygen species (ROS) [7]. The designed CPP-L/GelMA hydrogel was hoped to catalyze ROS by CAT in high ROS environment and trigger the hydrophilic change of PPS to release oxygen for a supplementary provision. Under normal conditions, the greater hydrophobicity of PPS block versus to the poly(propylene sulphide) block of poloxamers enhances the stability of the resulting vesicles. In the ROS environment, the sulphide in the PPS central block is partially oxidized to sulphoxides and eventually to sulphones, increasing the hydrophilicity of the initially hydrophobic

Fig. 2. Characterizations of composite hydrogels. (A) Schematic illustration of the CPP-L/GelMA hydrogel in ROS scavenging and intelligent oxygen supply. (B) Representative SEM image of the GelMA hydrogel and CPP-L/GelMA hydrogel. (C) The Young's modulus of hydrogels (n = 3). (D) Degradation of CPP-L/GelMA hydrogel under different conditions (n = 3). (E) Release of CAT from CPP-L/GelMA hydrogel under different conditions (n = 3). (F) Oxygen release rate of CPP-L/GelMA hydrogel (n = 3). (G) Oxygen release rate of CPP-L/GelMA hydrogel under different conditions (n = 3). Scale bars: 20 μm for GelMA and low magnification of CPP-L/GelMA in B, and 10 μm for high magnification of CPP-L/GelMA in B. *$p < 0.05$.

central block. This reaction induces morphological changes in highly stable vesicles from wormlike micelles to spherical micelles, and finally to unassociated monomolecular micelles, resulting in release of internal drugs [21]. We therefore evaluated the ROS responsive drug release of CPP-L/GelMA under H_2O_2 condition. As show in Fig. 2E and G, both the release rate of CAT and O_2 were apparently increased after the addition of H_2O_2 with 15 days. The increase of CAT release rate in ROS

environment may be due to ROS triggering PFC@PLGA/PPS particles to release oxygen, which then in turn stretching liposome and leading to the delivery of CAT. Many studies have shown that CAT, as an antioxidative enzyme, is responsible for catalyzing the dismutation of H_2O_2 into H_2O and O_2. CAT-L/GelMA also have good oxygen generation ability (7.5 mg/L), which accounts for about 40% of the total amount of oxygen supply of CPP-L/GelMA (Fig. S8). Therefore, the enhanced

oxygen supply was not only attributed to the fact that the CAT catalyzed H_2O_2 to improve the oxygen supply but also relied on the superfluous ROS responsive oxygen release from PFC@PLGA/PPS (Fig. 2A) [21,22].

3.2. CPP-L/GelMA hydrogel could facilitate angiogenesis in vitro

Although the CPP-L/GelMA hydrogel can provide a controlled-release of oxygen at the early stage of repair, the repair process of vessels and tissues is so long that the oxygen carried by the material can hardly meet the demand [23,57]. Therefore, it is necessary to rely on
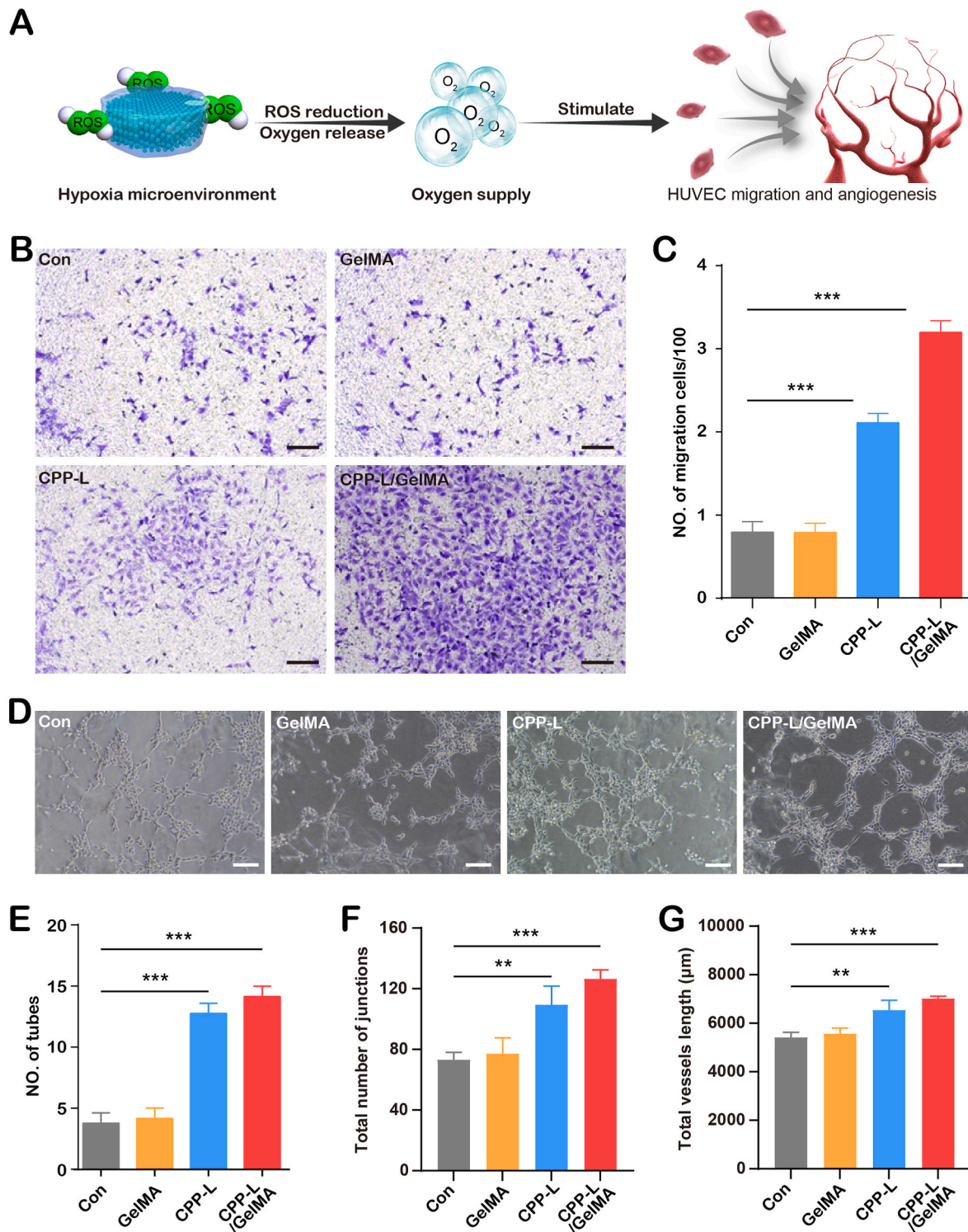
Fig. 3. CPP-L/GelMA hydrogel could facilitate angiogenesis *in vitro*. (A) Schematic illustration of the CPP-L/GelMA hydrogel in promoting angiogenesis. (B) Representative images of HUVECs migration in different treatments. (C) Statistics of migrated cell number (n = 3). (D) Representative images network formation in HUVECs of different groups. (E) Number of tubes in different treatments (n = 3). (F) Total number of junctions in different treatments (n = 3). (G) Total vessels length in different treatments (n = 3). Scale bars: 100 μm for B and C. $**p < 0.01$, $***p < 0.005$.

neovascularization to achieve long-term oxygen and nutrition supply. Fortunately, studies have found that increasing oxygen concentration can promote the formation of new blood vessels [58,59]. So theoretically, the CPP-L/GelMA hydrogel should be able to promote angiogenesis. Firstly, results of fluorescence staining and MTS assay revealed that the CPP-L/GelMA could promote the proliferation of HUVEC in hypoxic environment (Fig. S9), which was consistent with literature reports [60]. We then tested the effect of CPP-L/GelMA hydrogel on HUVEC migration. The results showed that the number of migrated cells in the CPP-L group was about 2-fold higher than that in the Control (Con) group and GelMA group, but still lower than that in the CPP-L/GelMA group (Fig. 3B and C). These results indicated that oxygen release could induce cell migration, and the persistence of oxygen release was directly proportional to the mobility of endotheliocyte. Then, a tube formation assay on Matrigel, which indicated the vascular capacity of endothelial cells, was performed to detect the angiogenesis of CPP-L/GelMA. It could be observed that in the two oxygen-releasing groups (CPP-L group and CPP-L/GelMA group), a large number of primary vascular-like network structure composed of tubular structures radiating from cell aggregates has been induced, and the number of tubes in CPP-L/GelMA group was more than that in CPP-L group. On the other hand, only incomplete tubes could be found in Con group and GelMA group (Fig. 3D and E). Moreover, the CPP-L/GelMA group exhibited the most outstanding results in total number of junctions (Fig. 3F) and total vessels length (Fig. 3G). These results demonstrated that continuous oxygen supply can effectively induce endothelial cells to form vascular like structures under a monotypic-cell and hypoxic environment in vitro (Fig. 3A).

3.3. Effects of CPP-L/GelMA hydrogel on osteoblasts and osteoclasts in vitro

Bone formation is closely related to the balance between osteoclasts and osteoblasts. Excessive bone loss is usually caused by the increased bone resorption carried out by osteoclasts or inhibition of osteoblasts which are related to the new bone formation [61]. Therefore, we explored the effects of CPP-L/GelMA hydrogel on osteoblasts and osteoclasts in vitro, so as to clarify the mechanism of the material in the process of bone regeneration (Fig. 4A).

3.3.1. CPP-L/GelMA hydrogel could scavenge ROS and promote osteogenic differentiation in vitro

Osteoblasts are differentiated from mesenchymal progenitor cells in the inner and outer periosteum or bone marrow matrix. Mature osteoblasts are monolayer cells located on the surface of bone, which are responsible for the synthesis, secretion and mineralization of bone matrix and affect the process of bone formation and reconstruction. Studies found that hypoxia and excessive ROS hypoxia could delay the growth and differentiation of osteoblasts [62–64]. This may be due to the reduced expression and activity of RUNX2 under such conditions, thereby reducing the differentiation of pluripotent mesenchymal cells into immature osteoblasts [65]. In this situation, increasing the oxygen supply of cells can reverse the trend [66].

In this study, we detected the effect of the CPP-L/GelMA hydrogel on ROS scavenging and osteogenic differentiation by co-culture of hydrogel and MC3T3-E1 cells in a hypoxic environment. As show in Fig. 4B, ROS levels (green fluorescence signal) in MC3T3-E1 cells with CPP-L/GelMA treatment were significantly decreased compared to control group, indicating that the oxidative stress state of MC3T3-E1 under hypoxia condition was significantly recovered by CPP-L/GelMA. Moreover, quantitative analysis showed that the expression of ROS in the CPP-L/GelMA group was down to 50% of that in the control (Con) group (Fig. 4C). Moreover, results of Western blot showed that at 10 days the CPP-L/GeLMA group held the highest expression levels of oxidative stress-related proteins NRF2 and HO-1, which were both about 2.5 times that of the Con group (Fig. 4D, G, and 4H). The CPP-L group also higher excellent expression levels of NRF2 and HO-1, but were still inferior to

that of the CPP-L/GelMA group which possessed better release characteristic of CAT and oxygen. Meanwhile, the highest expression level of RUNX2, which was one of the crucial transcription factors of osteogenic differentiation [67], could be found in the CPP-L/GelMA group (Fig. 4D and F). The CPP-L/GelMA group also showed absolute superiority in the expression of Col I, a major component of the extracellular matrix of bone tissue (Fig. 4D and E) [68]. These results showed that CPP-L/GelMA could do great help in scavenging ROS in MC3T3-E1 cells, which promoted the osteogenic differentiation in vitro.

In order to further verify the effect of CPP-L/GelMA on the whole osteogenic cycle, ALP staining and alizarin red staining were used to examine the osteogenic differentiation in the early stage and calcium nodule formation in the late stage respectively. After 7 days, it could be found that the number of ALP positive MC3T3-E1 cells in CPP-L group and CPP-L/GelMA group was significantly higher than that in Con group and GelMA group (Fig. 4I). Concurrently, the result of ALP staining in CPP-L/GelMA group was superior to that in CPP-L group, indicating a better ALP expression at the early stage of osteogenic differentiation. Alizarin red staining of cells after 21 days of induction showed a similar trend, in which the absorbance value at 562 nm in the CPP-L group was double higher than that of the Con group, while in the CPP-L/GelMA group that was even up to 4 times higher than that of the Con group (Fig. 4J and K). Additionally, the CPP-L/GelMA could obviously enhance the proliferation of MC3T3-E1 cells (Fig. S10). By these experiments it could be found that the ROS scavenging and continuous oxygen supply can promote the osteogenic differentiation of osteoblasts in hypoxic environment persistently and stably.

3.3.2. CPP-L/GelMA hydrogel could inhibit the differentiation of osteoclast in vitro

Osteoclasts are large multinucleated cells that are specifically used to absorb bone. Pre-osteoclasts from monocyte/macrophage lineages finally differentiate into mature cells with capability of absorbing bone, involving activation of nuclear factor-κB (RANK) receptor activator upon binding of its ligand (RANKL) [69]. Studies have shown that hypoxia can promote osteoclast differentiation and bone resorption in the presence of RANKL and M-CSF [70,71]. Further research showed that under hypoxic microenvironment the increase of osteoclast number was accompanied by the increase of gene and protein expression of osteoclast markers, including cathepsin K, matrix metalloproteinase-9, β3-integrin, calcitonin receptor, and TRAP [69,72].

In this study, we co-cultured different kinds of materials (GelMA, CPP-L, and CPP-L/GelMA) with RAW264.7 cells in hypoxic environment with osteoclast differentiation induction. The TRAP staining was then performed to observe the morphology and number of osteoclasts in each treatment (Fig. 4L and M). The results showed that the Con group and GelMA group held similar outcomes, as a large number of multinucleated giant cells indicating osteoclasts were observed. When it comes to the CPP-L group, due to the oxygen supply, the number of osteoclasts was reduced to half of the aforementioned 2 groups (Con group and GelMA group). While in the CPP-L/GelMA group, due to the further extension of oxygen supply time, osteoclasts were difficult to found and their size became much smaller than the CPP-L group. These results suggest that stable and continuous oxygen supply in hypoxic microenvironment has a significant inhibitory effect on osteoclasts.

3.3.3. CPP-L/GelMA hydrogel could promote osteogenic differentiation through BMAL1-autophagy pathway in vitro

Although oxygen delivery system is expected to improve the local hypoxic microenvironment and promote osteogenic differentiation, the relative specific mechanism has rarely been studied [2]. Exploring the internal mechanism is conducive to improving the cognition of the occurrence and development of the disease. Studies have shown that systemic stimuli (such as hormones, oxidative stress, and tissue local microenvironment) can affect the core clock transcription factor BMAL1 in the heart, which further affect the cell survival [73]. BMAL1 also
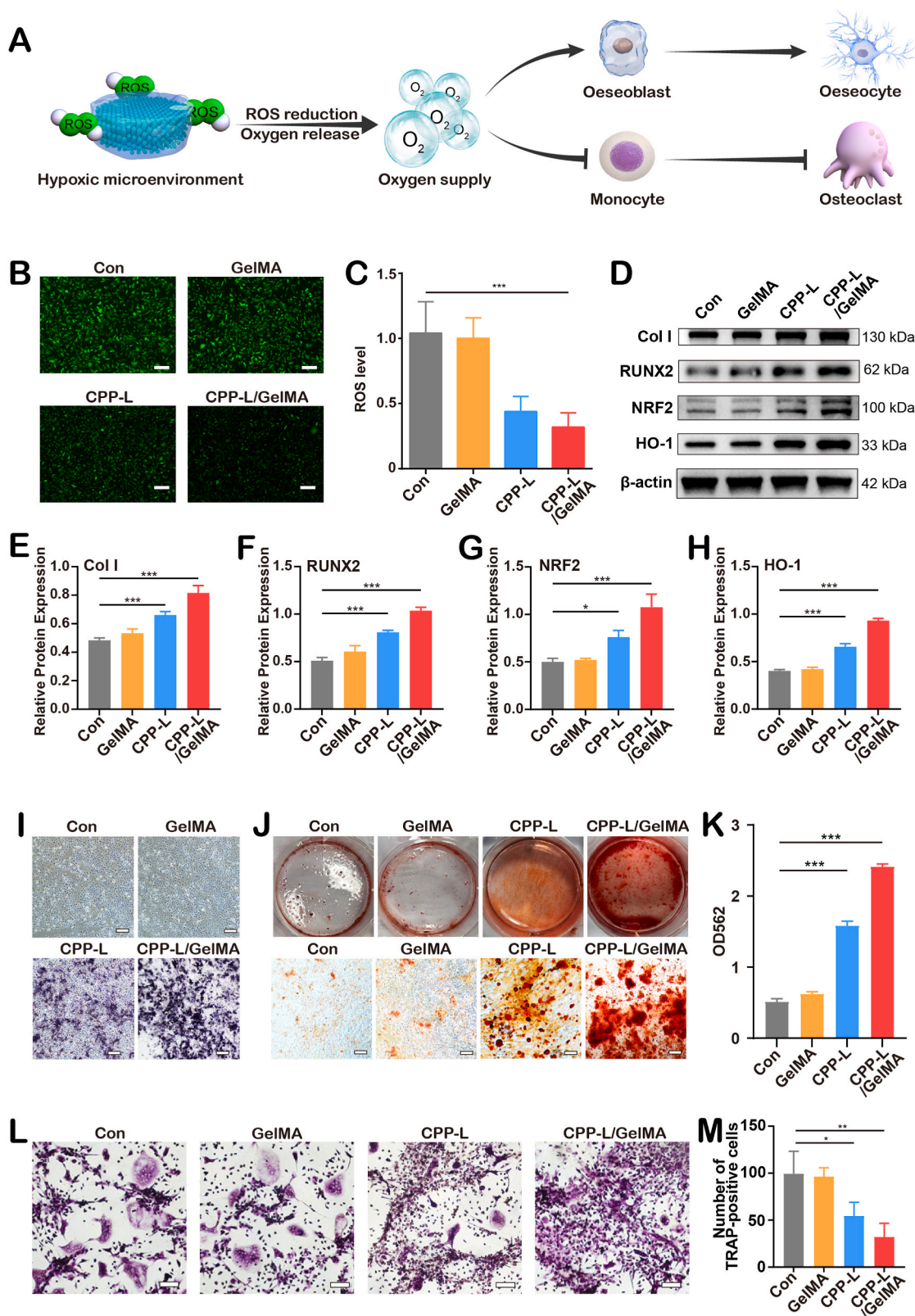
Fig. 4. Effects of CPP-L/GelMA hydrogel on osteoblasts and osteoclasts *in vitro*. (A) Schematic illustration of the CPP-L/GelMA hydrogel in promoting osteoblast differentiation while inhibiting osteoclasts formation. (B) Representative images of ROS fluorescence staining in MC3T3-E1 cells treated with different formulations. (C) Quantitative analysis of ROS fluorescence staining (n = 3). (D) Western blot of Col I, OPN, RUNX2, NRF2, HO-1, and β-actin protein levels of MC3T3-E1 differentiated osteoblast with different treatments. (E–H) Quantification analysis of the relative Col I (E), RUNX2 (F), NRF2 (G), and HO-1 (H) in MC3T3-E1 differentiated osteoblast with different treatments (n = 3). (I) Representative images of ALP staining of MC3T3-E1-differentiated osteoblast with different treatments. (J) Representative images of alizarin red staining of MC3T3-E1-differentiated osteoblast with different treatments. (K) Quantitative results of the alizarin red staining (n = 3). (L) Representative images of TRAP staining of RAW 246.7-differentiated osteoclasts with different treatments. (M) Statistics on the number of TRAP-positive cells (n = 3). Scale bars: 100 μm for B, I, J, and L. *$p < 0.05$, **$p < 0.01$, ***$p < 0.005$.

plays an important role in bone formation. BMAL1 deletion in BMSC inhibits osteoblast differentiation *in vitro*, while in osteoblasts with BMAL1 overexpression the expression of osteogenic related genes such as RUNX2 and OCN increased significantly [74]. It is worth noting that some studies have shown that the role of BMAL1 is not only limited to the regulation and oscillation of core clock genes, but also involved in maintaining redox homeostasis and improving cell survival under oxidative conditions [75,76]. On the other hand, ROS stress can reset the biological clock to coordinate survival promoting signals [77]. Thus, it can be seen that BMAL1 is closely related to ROS and oxidative stress. Moreover, BMAL1 can also play a positive role in many diseases by enhancing autophagy, and the relationship between autophagy and bone regeneration has also been confirmed in many studies [78]. Therefore, we hypothesize that our CPP-L/GelMA hydrogel may promote osteogenic differentiation through the regulation of BMAL1-autophagy pathway in the process of improving the hypoxic microenvironment.

In order to verify this inference, the Western blot (WB) has been performed on the MC3T3-E1 cells treated with GelMA, CPP-L, or CPP-L/GelMA under the induction of osteogenic differentiation. It could be observed that the hydrogels with oxygen releasing components, especially the CPP-L/GelMA group, could significantly enhance the expression of Col I (Fig. 5A and B) and OPN (Fig. 5A and C) in osteoblasts, which was consistent with the result of alizarin red staining. Subsequently, the expression level of BMAL1 protein in CPP-L group and CPP-L/GelMA group was significantly higher than that in the groups without oxygen releasing component (Con group and GelMA group) (Fig. 5A and D). The result of BMAL1 expression in CPP-L/GelMA group was even better than that in CPP-L group, indicating that the continuous correction of hypoxic microenvironment could indeed improve the expression level of BMAL1 in osteoblasts. Finally, we also detected the expression of NRF2, a key transcription factor of antioxidant stress [79], as well as the expression of autophagy related proteins in osteoblasts. The results showed that in the hypoxic environment, the expression level of NRF2 increased with the prolongation of oxygen supply time (Fig. 5A and E), indicating that the continuous oxygen supply of the hydrogel slowed down the oxidative stress of cells. Additionally, after oxygen administration in the CPP-L group and CPP-L/GelMA group, the up-regulation of autophagy effector protein Beclin1 could be observed (Fig. 5A and F), and the ratio between LC3 II and LC3 I also increased significantly (Fig. 5A and G). During the formation of autophagy, cytoplasmic LC3 (LC3 I) could be enzymatically digested into a small segment of polypeptide and change into autophagosome membrane type (LC3 II). Thus, the increased ratio of LC3-II/I indicated the enhancement of autophagy level in MC3T3-E1 cells. These results suggested that the CPP-L/GelMA hydrogel could restore the BMAL1 expression of osteoblast, and simultaneously improve the autophagy and osteogenic potential of cells.

To further clarify the regulatory effect of BMAL1 on autophagy, we concurrently transfected an siRNA against BMAL1 into MC3T3-E1 under hypoxic microenvironment (Fig. 5). When BMAL1 was inhibited, the expressions of Beclin1 and LC II/I were significantly decreased (about 50%) in all groups after various kinds of materials treatment, indicating that BMAL1 has a regulatory effect on MC3T3-E1 autophagy in this process. Moreover, the osteogenic differentiation of cells was also inhibited after the transfection of the siRNA, as the expression levels of Col I and OPN decreased significantly in all groups. Among them, the expression of Col I and OPN in the siRNA[BMAL1]/CPP-L/GelMA group was about a half of that in CPP-L/GelMA group. Subsequently, we also confirmed the aforementioned relationship between BMAL1 and the osteogenesis related protein under a hypoxic microenvironment by immunofluorescence staining. The results showed that the fluorescence intensity of BMAL1 and osteogenic related protein RUNX2 increased significantly in the CPP-L group and CPP-L/GelMA group, while the expression level of RUNX2 accordingly decreased after BMAL1 inhibition (Fig. 5H, S11, and S12). All these results preliminarily showed that efficient and continuous oxygen supply could significantly improve the

BMAL1 expression of osteoblasts in hypoxic microenvironment, and in turn improve the efficiency of osteogenic differentiation by enhancing the autophagy (Fig. 5I).

3.4. CPP-L/GelMA hydrogel can relieve hypoxia and scavenge ROS in the site of bone defect in vivo

After implementing the mouse skull defect model and implanting the CPP-L/GelMA hydrogel, we used ROS Brite™ 700, Hypoxyprobe, and immunohistochemistry to detect hypoxic levels, ROS scavenging, and periosteal NRF2 expression each time point (Fig. 6A).

Studies have proved that the rupture of blood vessels at the fracture site can lead to local hypoxia, and disuse can also aggravate osteocyte hypoxia in a reversible way [80,81]. Moreover, increasing evidence has shown that the hypoxic microenvironment in bone defect areas induces oxidative stress in cells, while ROS and endogenous antioxidant defense system are involved in the fate determination and functional regulation of bone-related cells [82]. We primarily detected ROS levels in mouse skull defects by using the ROS Brite™ 700 probe. The results of *in vivo* imaging (Fig. 6B) revealed that the cells in the bone defect area were indeed in a state of oxidative stress, and the ROS level was maintained at a high level during the subsequent process. The ROS level in GelMA group was lower than that in Con group in 2–4 weeks of regeneration, probably because the GelMA hydrogels provided space to support the growth and extension of vessel [83], which increased oxygen supply. Therefore, the ROS environment in the bone defect area of the GelMA group was easier to be alleviated. On the other hand, the CPP-L and CPP-L/GelMA significantly reduced ROS levels in bone defect after 1 week of implantation, and kept decreasing in a time-dependent manner. Among all the groups, the CPP-L/GelMA group showed the most outstanding ROS scavenging ability, with the ROS level being 1/2 of the Con group at 1 week and only 1/8 of the Con group at 6 weeks (Fig. 6C). These findings suggest that cells in bone defect areas are under a high level of oxidative stress, which can be effectively scavenged by the CPP-L/GelMA hydrogel.

The Hypoxyprobe was used to evaluate whether implantation of CPP-L/GelMA hydrogel could improve the hypoxic microenvironment at bone defect sites (Fig. 6D). First, our experiment confirmed that cells in the bone defect area are anoxic, which was consistent with previous literature [84], as high levels of Hypoxyprobe signal were detected in tissue sections of cranial defect sites in the Con group at 4 weeks. However, quantitative analysis of the Hypoxyprobe signal showed that relative fluorescence intensity in the skull defect area of mice implanted with CPP-L/GelMA hydrogel was significantly reduced compared with the Con group (Fig. 6E). Although the GelMA and CPP-L were observed to partly alleviate the hypoxic microenvironment of bone defects as well, there still exist disparity when compared with the CPP-L/GelMA group. The difference between the GelMA group and CPP-L/GelMA group was mainly due to the responsive purification effect of the CPP-L in CPP-L/GelMA group on hypoxic environment, while the higher expression of Hypoxyprobe in CPP-L group compared with CPP-L/GelMA group indicate that the rapid release of oxygen would affect the durability of the improvement of hypoxic microenvironment. An interesting phenomenon could be found after concurrently analyzing of the results of ROS and hypoxia, that the relative ROS level of CPP-L/GelMA was much lower than the relative expression level of Hypoxyprobe signal at 4 weeks. This may be because the CPP-L/GelMA significantly reduced the ROS level in bone defect site so that the ROS-responsive oxygen production is relatively weakened, reflecting that our hydrogel was also ROS-responsive *in vivo*. Our results revealed that the outstanding responsive oxygen-production characteristics of CPP-L/GelMA hydrogel could effectively improve the hypoxic microenvironment in the skull defect area of mice.

In addition, we have also performed oxygen measurement experiment to evaluate the ROS-responsive oxygen-generation *in vivo*. After implanted the CPP-L/GelMA hydrogel in mouse skull defect model, we
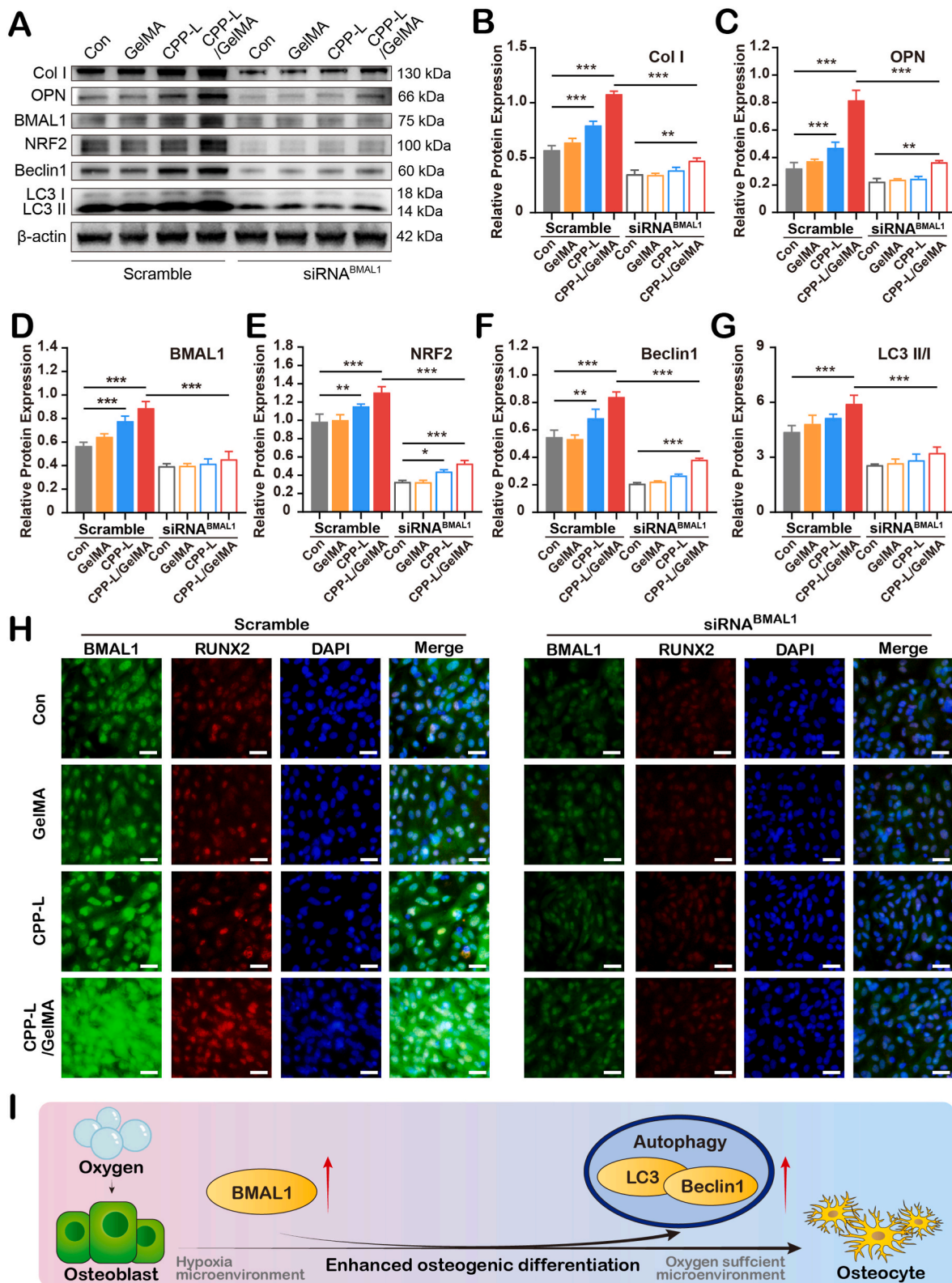
Fig. 5. CPP-L/GelMA hydrogel could promote osteogenic differentiation through BMAL1-autograhpy pathway *in vitro*. (A) Western blot of Col I, OPN, BMAL1, NRF2, Beclin1, LC3 I and LC3 II, and β-actin protein levels of MC3T3-E1-differentiated osteoblast with different treatments. (B–G) Quantification analysis of the relative Col I (B), OPN (C), BMAL1 (D), NRF2 (E), Beclin1 (F), and LC3 II/I (G) in MC3T3-E1 differentiated osteoblast with different treatments (n = 3). (H) Representative images of BMAL1 and RUNX2 immunofluorescence staining on MC3T3-E1-differentiated osteoblast with different treatments at day 7. (I) Schematic illustration of bone microenvironment regulative hydrogels CPP-L/GelMA promoting the osteogenic differentiation of osteoblasts through activating the BMAL1-autophagy pathway. Scale bars: 50 μm for H. **$p < 0.01$, ***$p < 0.005$.
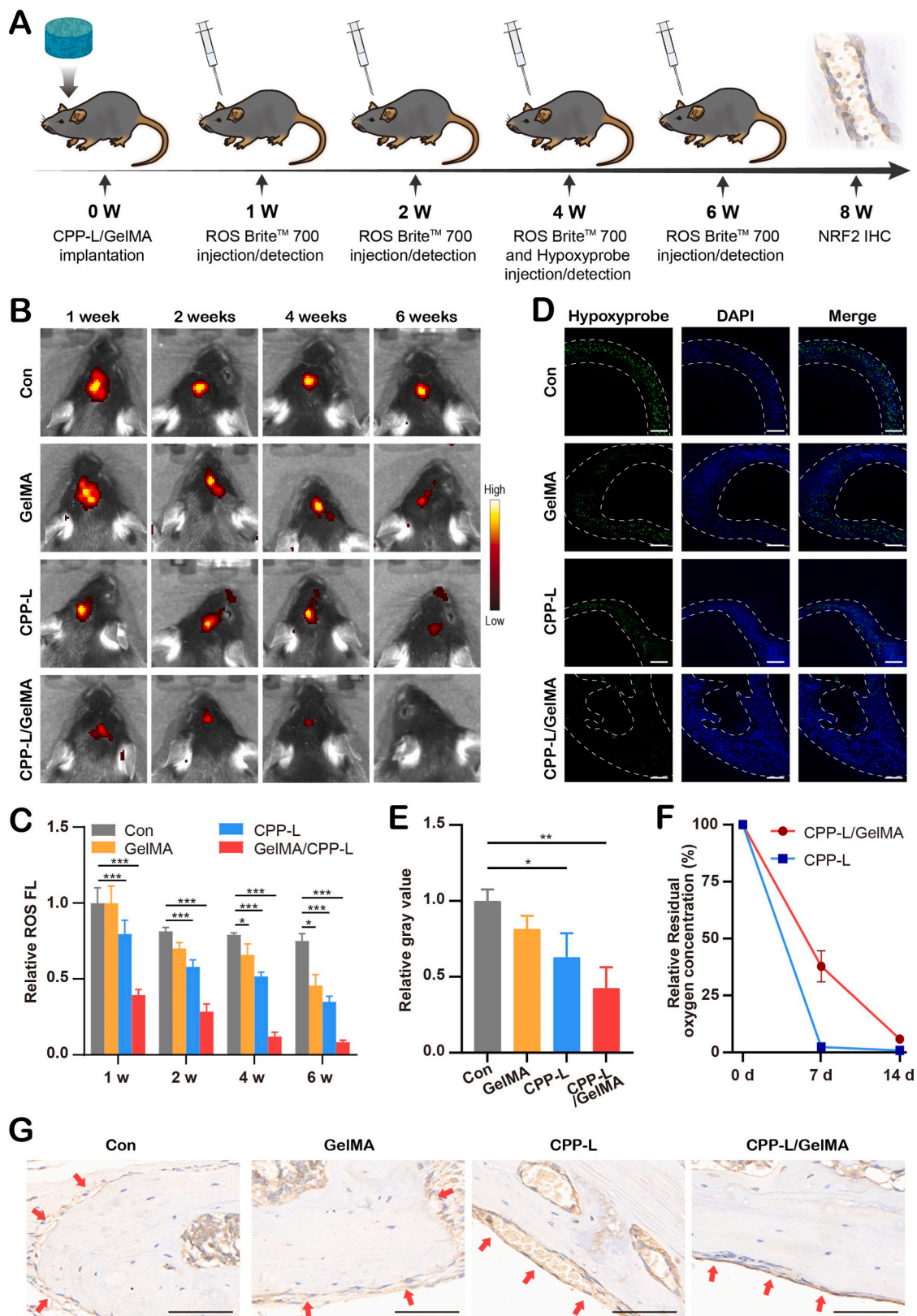
Fig. 6. CPP-L/GelMA hydrogel can relieve hypoxia and scavenge ROS in the site of bone defect *in vivo*. (A) Schematic illustration of the time line for treatment monitoring. (B) Representative images of *in vivo* imaging system at different time points after injection of ROS Brite™ 700. (C) Quantification analysis of the ROS Brite™ 700 (n = 6). (D) Representative fluorescence images of skull defect area at 4 weeks after injection of Hypoxyprobe. (E) Quantification analysis of the Hypoxyprobe staining (n = 3). (F) Relative residual oxygen concentration in implanted CPP-L or CPP-L/GelMA. (G) Representative immunohistochemical staining images of NRF2 of skull defect region from mice after different treatments at 8 weeks (the red arrow points to the periosteum where the osteoblasts are located). Scale bars: 200 μm for C and 50 μm for F. *$p < 0.05$, **$p < 0.01$, ***$p < 0.005$.

collected the CPP-L/GelMA hydrogel at different time points to measure the residual oxygen concentration under H_2O_2 condition by using oxygen probe to determine the oxygen release *in vivo*. As show in Fig. 6F, CPP-L/GelMA could continuously generate oxygen for more than two weeks in mouse skull defect model, which indicated that the hypoxia condition *in vivo* could promote the persistent and stable oxygen generation of CPP-L/GelMA.

The NRF2 is a key gene in redox regulation, which plays an important role in combating oxidative stress [85,86]. In addition to reflecting ROS levels, study has shown that the expression level of NRF2 is also related to the hypoxia of cells [87]. Therefore, the expression of NRF2 in the periosteum of newly formed bone, which mainly contained osteoblasts [88], was detected by the immunohistochemistry (Fig. 6G). The results showed that the expression of NRF2 was both low in the periosteum of Con and GelMA groups. On the contrary, numerous positive osteoblasts could be observed in the CPP-L group and the CPP-L/GelMA group, and the NRF2 expression level of the CPP-L/GelMA group was much superior. Study of Sun et al. showed a similar result [87]. They found that the expression of NRF2 in bone marrow mesenchymal stem cells (BMSC), the precursor cell of osteoblast, was inhibited under hypoxia, which further affected the activity of BMSC through NQO-1 and HO-1. The trends of NRF2 coincided with those of ROS and Hypoxyprobe signaling pathway, indicating that CPP-L/GelMA hydrogel could effectively scavenge ROS and improve hypoxic microenvironment *in vivo*, laying a foundation for subsequent bone regeneration.

3.5. CPP-L/GelMA hydrogel can effectively promote osteogenesis and angiogenesis in vivo

In order to explore the ability of CPP-L/GelMA hydrogel to repair bone defects, we constructed a mice skull defect model (Fig. 7A) and used micro-CT to detect bone regeneration at 4 and 8 weeks after implantation. The results, as exhibited in Fig. 7B, showed that the areas of bone defects in the GelMA group, CPP-L group, and CPP-L/GelMA group were all decreased at 8 weeks compared with that at 4 weeks. The reduction in Con group was the smallest, which mainly reflected in the change of new bone tissue from granular newly formed bone at 4 weeks to cortical bone at 8 weeks. On the contrary, besides the change of tissue texture, the expansion of new bone was also the most obvious in the CPP-L/GelMA group. Subsequently, we used bone volume fraction (BT/TV) and bone mineral density (BMD) to further quantitatively analyze the formation of new bone in each group. Through the BV/TV it could be more clearly observe that the growth rate of bone tissue at the defect site in the CPP-L/GelMA group was the fastest, while that in the Con group was the slowest (Fig. 7C). At 8 weeks, the percent bone volume in CPP-L/GelMA group was about 3 times higher than that in Con group with significant statistical difference ($P < 0.005$). In addition to the bone volume fraction, we also analyzed BMD the quality of new bone (Fig. 7D). The statistical results showed that BMD in GelMA group were better than those in Con group. The CPP-L group showed higher density than the two oxygen-free groups (Con group and GelMA group), but was still inferior to the CPP-L/GelMA group. It is worth noting that the results of micro-CT in GelMA group are better than those in Con group *in vivo*, which are different from the results of *in vitro* experiments. We attribute this phenomenon to the speculation that in a multicellular and multi growth factor environment *in vivo* the GelMA hydrogel, despite without any modification, could exhibit osteoconductivity and provide a space for cells proliferation, which ultimately leads to a better result than the Con group [89]. Overall, relying on the ROS scavenging and continuous oxygen supply, the CPP-L/GelMA hydrogel can effectively promote the bone regeneration *in vivo*, and the newly formed bone possesses excellent mineral density.

Subsequently, a H&E staining was performed at 8 weeks to further observe the histomorphology of bone defect in each group after repairing. Numerous newly formed bone could be observed in GelMA group, CPP-L group, and CPP-L/GelMA group, in which the CPP-L/GelMA group held the best result of new bone formation (Fig. 7E). Interestingly, although bone growth could be observed in all the three groups with material implantation, the growth direction of the CPP-L group was different from that of GelMA group or CPP-L/GelMA group. In the CPP-L group, bone tissue tended to grow vertically instead of horizontally. This may be due to the lack of large scaffolds in CPP-L group, which can hardly provide horizontal osteoconductivity [89,90]. Concurrently, the osteoinductivity provided by ROS scavenging and oxygen supply resulted in the growth of a certain amount of new bone tissues along the vertical direction.

Angiogenesis is an important part during bone regeneration. We have preliminarily detected the ability of materials to promote angiogenesis *in vitro*. In order to further verify the reliability of these results, we also characterized the angiogenesis of the skull defect in mice. CD31 is a highly glycosylated Ig like membrane receptor expressed by leukocytes, platelets, and endothelial cells, currently being the most abundant membrane glycoprotein constructively expressed on vascular endothelial cells [91]. At present, CD31 is often used as a marker to identify tissue vascular endothelium. In this study, we used CD31 immunohistochemistry to observe the *in vivo* angiogenesis. The results showed that the number of newly formed blood vessels in the bone defect area in the two oxygen-releasing groups was significantly higher than that in other two groups. Additionally, the mean number of blood vessels in CPP-L/GelMA group was 1.5 times that in CPP-L group (Fig. 7F and G). In order to further verify these results, we also performed Flk-1 immunofluorescence staining on the samples. Flk-1, which is also called vascular endothelial growth factor receptor 2, exists in the endothelium of blood vessels and lymphatic vessels and plays a regulatory role in the formation of these two tissues [92,93]. Through the immunofluorescence staining it can be observed that the CPP-L/GelMA group still achieved the best outcome (Fig. 7I), the relative gray value of which was about 30% higher than that of Con group with significant statistic difference ($p < 0.01$) (Fig. 7H). These results indicates that ROS scavenging and oxygen supply at the defect site can promote angiogenesis, and the longer action time can stimulate more blood vessels formation, which were consist with previous literatures and clinical impression [18,59,94, 95]. Additionally, a murine subcutaneous implantation model was used to evaluate degradation of CPP-L/GelMA *in vivo* [96]. Explanted CPP-L/GelMA and GelMA hydrogels decreased consistently until day 21 (Fig. S13), indicated the good degradation ability of CPP-L/GelMA *in vivo*. It has also been found that the CPP-L/GelMA hydrogel held good *in vivo* biosafety (Fig. S14 and Table S1).

3.6. CPP-L/GelMA hydrogel promotes bone regeneration in vivo by upregulated BMAL1 and autophagy

Finally, we preliminarily explored the expression of BMAL1 and autophagy in bone tissue at the defect site *in vivo*. Because osteoblasts are generally distributed in the periosteum on the surface of new bone *in vivo*, we therefore investigated the expression of osteoblast related proteins in the periosteum of newly formed bone tissue [88]. Results of immunohistochemistry showed that the number of BMAL1 positive cells in periosteum of CPP-L/GelMA group were more than that of CPP-L group, Con group and GelMA group (Fig. 8A). The immunofluorescence staining also revealed a similar trend about the expression of BMAL1 in newly formed bone tissue (Fig. 8B and C), indicating that our oxygen-releasing hydrogel could improve the expression of BMAL1 genes in osteoblasts.

Subsequently, we also explored the autophagy of osteoblasts *in vivo* by the immunohistochemistry. As shown in Fig. 8A, the number of LC3 positive cells in periosteum of GelMA group was more than that of Con group. Although the number of positive cells in CPP-L group was more than that in the two non-oxygen releasing group, it was still less than that in CPP-L/GelMA group due to the rapid release of oxygen (Fig. 8A). To further verify the accuracy of these results, we also performed the Beclin1 immunofluorescence staining. Beclin1 is an essential molecule
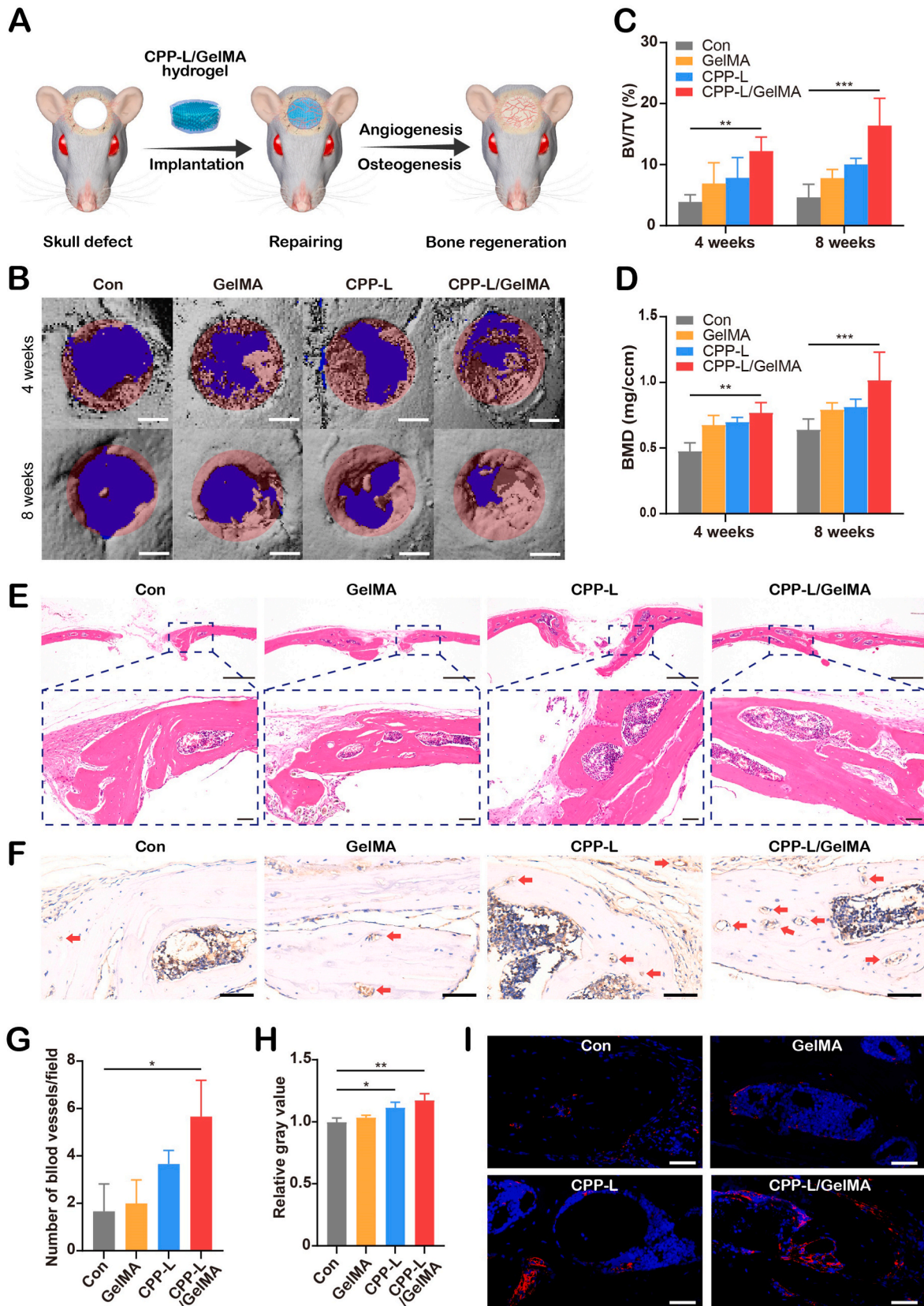
(caption on next page)

Fig. 7. CPP-L/GelMA hydrogel could promote osteogenesis and angiogenesis *in vivo*. (A) Schematic illustration of the CPP-L/GelMA hydrogel implantation into the area of mice skull defect for enhancing bone repair. (B) Representative 3D reconstruction micro-CT images of skull defect region from mice after different treatments at 4 weeks and 8 weeks (the red circle indicates the range of original bone defect). (C–D) Calculated bone volume fraction (C) and bone mineral density (D) of skull defect region from mice after different treatments (n = 3). (E) Representative images of H&E staining of skull defect region from mice after different treatments at 8 weeks (the second row represents higher magnification images (200 ×) of the corresponding black square boxes in the upper row (40 ×). (F) Representative immunohistochemical staining images of CD31 of skull defect region from mice after different treatments at 8 weeks (the red arrow shows the blood vessel). (G) Quantitative analysis of vessel density based on the CD31 immunohistochemical staining (n = 3). (H) Quantification analysis of the Flk-1 immunofluorescence staining (n = 3) of skull defect region from mice after different treatments. (I) Representative images of Flk-1 immunofluorescence staining of skull defect region from mice after different treatments at 8 weeks. Scale bars: 500 μm for B and the upper row of E; 50 μm for the second row of E, F, and I. $*p < 0.05$, $**p < 0.01$, $***p < 0.005$.

for the formation of autophagosomes, which can mediate the localization of autophagy related proteins in phagocytic vesicles and react with a variety of proteins to regulate the formation and maturation of autophagosomes [97]. It can be found that the number and intensity of red fluorescence in the CPP-L/GelMA group was more than that of the other 3 groups (Fig. 8B). The relative gray value of CPP-L/GelMA group was about 1.8 times that of the Con group, and was about 15% higher than that of the CPP-L group, indicating the Beclin1 expressed by osteoblast in CPP-L/GelMA group with long-term oxygen administration were significantly higher than those in non-oxygen groups (Con group and GelMA group) and the oxygen burst release group (CPP-L group) (Fig. 8B and D). These results represent that after the purification conducted by the CPP-L/GelMA hydrogel, the reverse of hypoxic microenvironment significantly increased the autophagy level of osteoblasts in newly formed bone.

The improvement of BMAL1 expression and autophagy caused by continuous oxygen administration played a positive role in bone formation, as evidence of the up-regulated expression of Col I of the CPP-L/GelMA group observed through the immunohistochemistry (Fig. 8A). Through OPN immunofluorescence staining, a large number of cord-like green fluorescence could be observed in the CPP-L/GelMA group, which constructed a lamellar bone like structure. Correspondingly, there was much less cord-like green fluorescence in the CPP-L group and GelMA group, while almost no similar fluorescence could be found in the Con group (Fig. 8B). The result of quantitative analysis showed that the ratio between the CPP-L/GelMA group and Con group was about 2:1 (Fig. 8E), indicating an outstanding outcome of the CPP-L/GelMA in inducing osteogenic differentiation *in vivo*.

All these results preliminarily proved that the CPP-L/GelMA hydrogel can improve the local hypoxic microenvironment in the site of bone defect by continuous ROS scavenging and oxygen supply, thereby improving the expression of BMAL1 genes in osteoblasts, and further enhancing autophagy to promote bone regeneration (Fig. 8F). At present, most studies considered that hypoxia microenvironment regulates bone regeneration through the hypoxia-inducible transcription factors (HIF) signal pathway [98]. Through this study it has been demonstrated that the novel BMAL1-autophagy pathway was also one of the key elements for the regulation of environmental oxygen content on osteogenesis. Regrettably, this study failed to expound the direct connections between BMAL1 and oxygen related functions. Peek et al. found that under hypoxia conditions, the gene destruction of BMAL1 in skeletal muscle tubes and fibroblasts increased the level of hypoxia inducible factor-1 α (HIF1 α) [99], while Wu et al. proposed that the clock plays functions in fine-tuning hypoxic responses under pathophysiological conditions [100]. In the subsequent studies, we will conduct in-depth research on oxygen-BMAL1.

Recently, several studies have been devoted to the fabrication of oxygen-releasing scaffolds, but the release rate of oxygen in these scaffolds was so fast that most of them were used in the treatment of wounds [32–34]. The process of bone regeneration is much longer [101]. Our experiments also showed that the ROS level in mouse skull defects region was maintained at a high level within 6 weeks (Fig. 6B). Although some oxygen-producing scaffolds have been used in bone defect repair and achieved promising results, there still remains the problem of short oxygen-releasing time [84]. Hence, we designed the ROS scavenging

and responsive prolonged oxygen-generating hydrogels (CPP-L/GelMA) as a bone microenvironment regulator to reverse the hypoxic microenvironment in bone defects region. Under hypoxic condition, CPP-L/GelMA can release CAT for degrading hydrogen peroxide to generate oxygen and be triggered by superfluous ROS to continuously release the oxygen for more than 2 weeks both *in vitro and in vivo*, which finally significantly enhanced angiogenesis and osteogenesis in skull defect area as previously showed.

In the future, we intend to further improve our system to achieve more sustained oxygen release through photocontrol or responsive degradation. Moreover, loading bone marrow mesenchymal stem cells into the hydrogel is also expected to further increase the repair effect of the system. There have been a certain number of studies that revealed promising therapeutic outcomes through stem cell delivery systems [102,103]. However, cells obtention generally requires invasive harvesting, along with uncertain survival rate [104]. Therefore, we are more expectation to fabricate novel bone regenerative material which can restore, recruit, and mobilize the body's own stem cells.
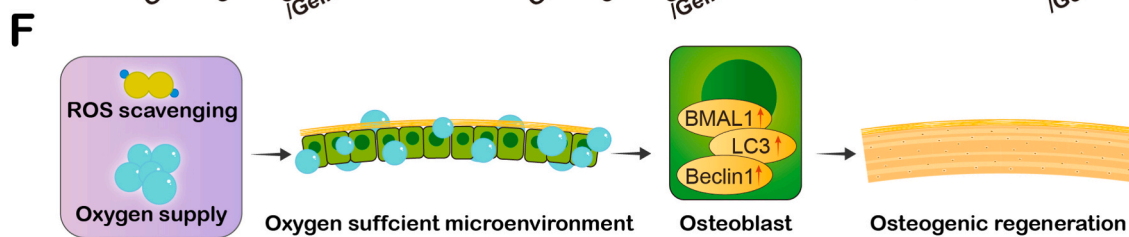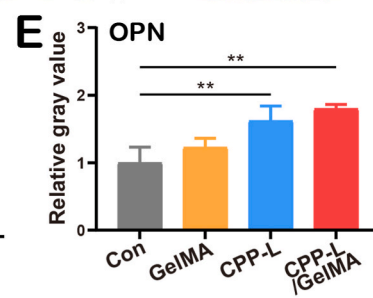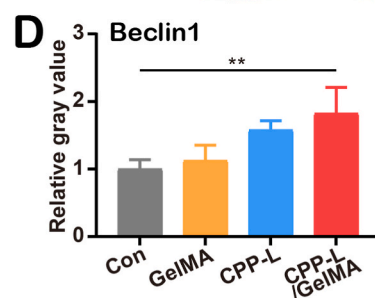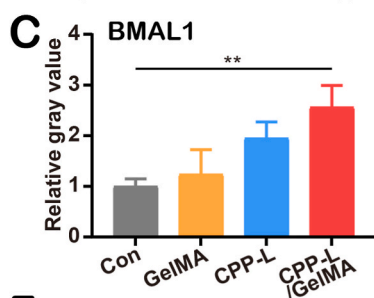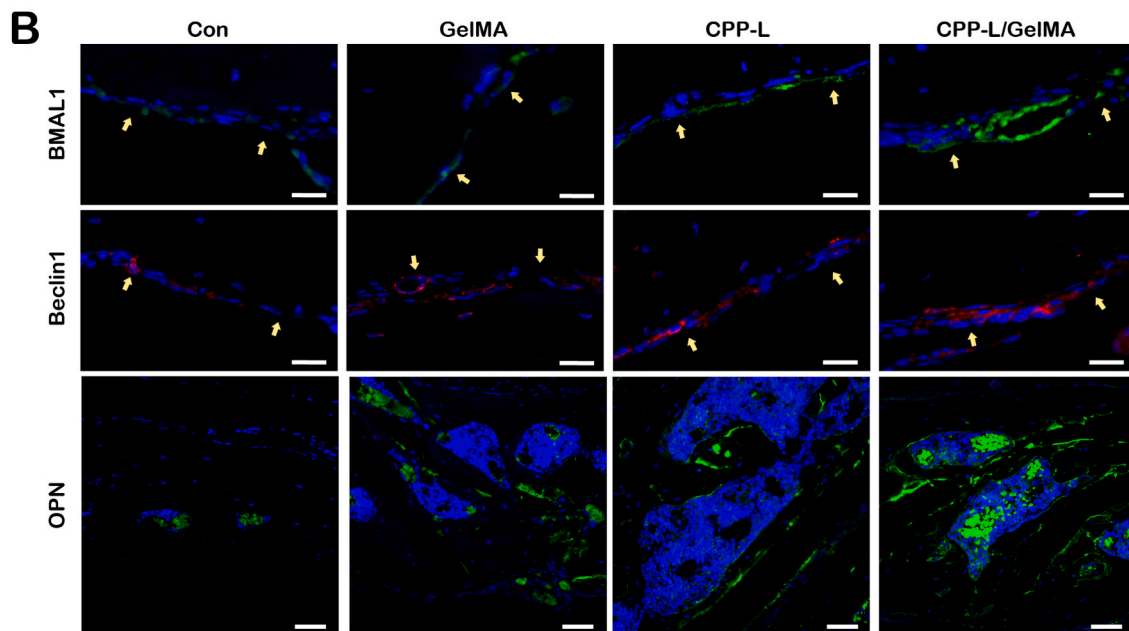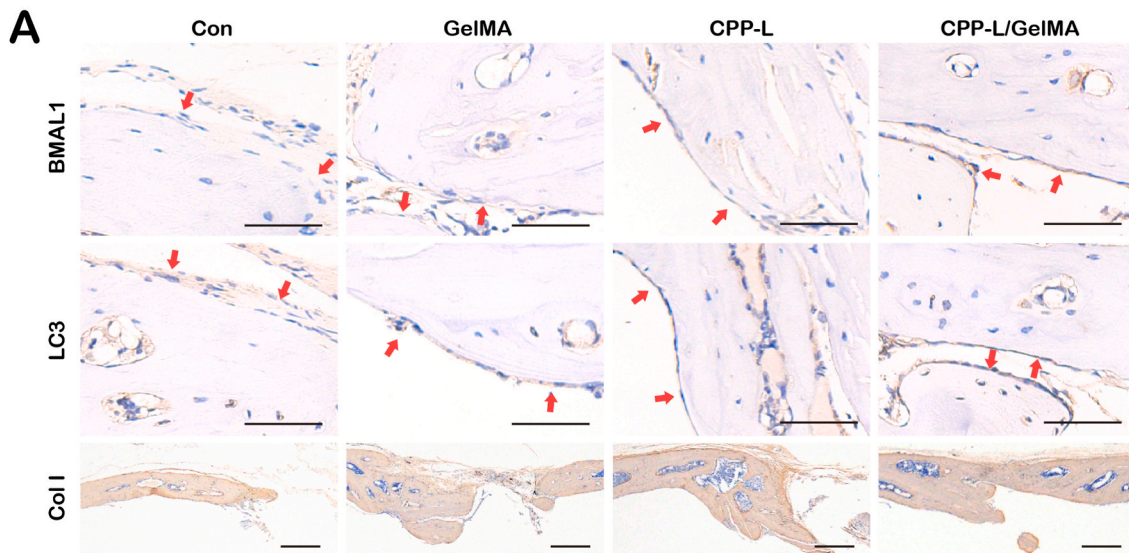
4. Conclusion

In summary, we developed an intelligent responsive oxygen-releasing hydrogel. The CPP-L/GelMA hydrogel, which acts as a microenvironment regulator during for bone tissue respiration, can delivery CAT to enzymatic hydrolyze the ROS in the hypoxic microenvironment of bone defects to form oxygen. Concurrently, the superfluous ROS can trigger the hydrophilic change of PPS, which locates on the surface of oxygen-carrying nanoparticles in hydrogel, to release oxygen so as to further improve the oxygen supply according to environmental requirements. The formation of oxygen enriched microenvironment promotes the formation of neovascularization and inhibits the formation of osteoclasts. More importantly, adequate oxygen supply can improve the expression of BMAL1 gene in osteoblasts, which further promote osteogenic differentiation by enhancing autophagy, and finally significantly facilitate the bone regeneration. Therefore, the engineered novel oxygen-supply CPP-L/GelMA hydrogel is expected to provide a new and effective treatment strategy for clinical critical size bone defects.

Ethics approval and consent to participate

The experimental protocol was established, according to the ethical guidelines of the Helsinki Declaration and was approved by the Ethics Committee of the Drum Tower Hospital, Medical School of Nanjing University.

CRediT authorship contribution statement

Han Sun: Experiments, Data curation, Writing – original draft. **Juan Xu:** Data curation, Formal analysis. **Yangyufan Wang:** Data curation, Formal analysis. **Siyu Shen:** Data curation, Formal analysis. **Xingquan Xu:** Investigation, Data curation, Formal analysis, Conceptualization. **Lei Zhang:** Investigation, Data curation, Formal analysis, Conceptualization, Supervision. **Qing Jiang:** Investigation, Data curation, Formal analysis, Conceptualization, Supervision.

A

B

C BMAL1

D Beclin1

E OPN

F
ROS scavenging / Oxygen supply → Oxygen suffcient microenvironment → Osteoblast (BMAL1↑, LC3↑, Beclin1↑) → Osteogenic regeneration

(caption on next page)

Fig. 8. CPP-L/GelMA hydrogel promotes osteogenesis *in vivo* by upregulated BMAL1 and autophagy. (A) Representative images of BMAL1, LC3, and Col I immunohistochemical staining of skull defect region from mice after different treatments at 8 weeks (the red arrow points to the periosteum where the osteoblasts are located). (B) Representative images of BMAL1, Beclin1, and OPN immunofluorescence staining of skull defect region from mice after different treatments at 8 weeks (the yellow arrow points to the periosteum where the osteoblasts are located). (C–E) Quantification analysis of the BMAL1 (C), Beclin1 (D), and OPN (E) immunofluorescence staining of skull defect region from mice after different treatments (n = 3). (F) Schematic illustration of ROS scavenging and oxygen supply in the hypoxic microenvironment of skull defect region in promoting osteogenic regeneration through activating the BMAL1-autophagy pathway *in vivo*. Scale bars: 50 μm for the BMAL1 and LC3 in A, and OPN in B; 200 μm for Col I in A; 20 μm for BMAL1 and beclin1 in B. **$p < 0.01$.

Declaration of competing interest

The authors declare that they have no conflicts of interests.

Appendix A. Supplementary data

Supplementary data to this article can be found online at https://doi.org/10.1016/j.bioactmat.2022.12.021.

References

[1] Y. Xu, C. Xu, L. He, J. Zhou, T. Chen, L. Ouyang, X. Guo, Y. Qu, Z. Luo, D. Duan, Stratified-structural hydrogel incorporated with magnesium-ion-modified black phosphorus nanosheets for promoting neuro-vascularized bone regeneration, Bioact. Mater. 16 (2022) 271–284, https://doi.org/10.1016/j.bioactmat.2022.02.024.

[2] S.W. Teh, A.E. Koh, J.B. Tong, X. Wu, A.V. Samrot, S. Rampal, P.L. Mok, S.K. Subbiah, Hypoxia in bone and oxygen releasing biomaterials in fracture treatments using mesenchymal stem cell therapy: a review, Front. Cell Dev. Biol. 9 (2021), 634131. https://10.3389/fcell.2021.634131.

[3] S. Suvarnapathaki, X. Wu, T. Zhang, M.A. Nguyen, A.A. Goulopoulos, B. Wu, G. Camci-Unal, Oxygen generating scaffolds regenerate critical size bone defects, Bioact. Mater. 13 (2022) 64–81, https://doi.org/10.1016/j.bioactmat.2021.11.002.

[4] M. Ejtehadifar, K. Shamsasenjan, A. Movassaghpour, P. Akbarzadehlaleh, N. Dehdilani, P. Abbasi, Z. Molaeipour, M. Saleh, The effect of hypoxia on mesenchymal stem cell biology, Adv. Pharmaceut. Bull. 5 (2) (2015) 141–149. https://10.15171/apb.2015.021.

[5] S. Stegen, I. Stockmans, K. Moermans, B. Thienpont, P.H. Maxwell, P. Carmeliet, G. Carmeliet, Osteocytic oxygen sensing controls bone mass through epigenetic regulation of sclerostin, Nat. Commun. 9 (1) (2018), 2557-2557, https://10.1038/s41467-018-04679-7.

[6] Y.C. Huang, H.M. Zhu, J.Q. Cai, Y.Z. Huang, J. Xu, Y. Zhou, X.H. Chen, X.Q. Li, Z.M. Yang, L. Deng, Hypoxia inhibits the spontaneous calcification of bone marrow-derived mesenchymal stem cells, J. Cell. Biochem. 113 (4) (2012) 1407–1415. https://10.1002/jcb.24014.

[7] J.Y. Li, F.X. Han, J.J. Ma, H. Wang, J. Pan, G.B. Yang, H. Zhao, J.Y. Zhao, J.B. Liu, Z. Liu, B. Li, Targeting endogenous hydrogen peroxide at bone defects promotes bone repair, Adv. Funct. Mater. 32 (10) (2022) 2111208. https://10.1002/adfm.202111208.

[8] N. Mody, F. Parhami, T.A. Sarafian, L.L. Demer, Oxidative stress modulates osteoblastic differentiation of vascular and bone cells, Free Radic. Biol. Med. 31 (4) (2001) 509–519. https://10.1016/s0891-5849(01)00610-4.

[9] D.H. Lee, B.S. Lim, Y.K. Lee, H.C. Yang, Effects of hydrogen peroxide (H2O2) on alkaline phosphatase activity and matrix mineralization of odontoblast and osteoblast cell lines, Cell Biol. Toxicol. 22 (1) (2006) 39–46. https://10.1007/s10565-006-0018-z.

[10] T. Okamoto, M. Taguchi, T. Osaki, S. Fukumoto, T. Fujita, Phosphate enhances reactive oxygen species production and suppresses osteoblastic differentiation, J. Bone Miner. Metabol. 32 (4) (2014) 393–399. https://10.1007/s00774-013-0516-z.

[11] D. Lee, K.J. Shin, D.W. Kim, K.A. Yoon, Y.J. Choi, B.N.R. Lee, J.Y. Cho, CCL4 enhances preosteoclast migration and its receptor CCR5 downregulation by RANKL promotes osteoclastogenesis, Cell Death Dis. 9 (5) (2018) 495. https://10.1038/s41419-018-0562-5.

[12] S.J. Woo, H.S. Noh, N.Y. Lee, Y.H. Cheon, S.M. Yi, H.M. Jeon, E.J. Bae, S.I. Lee, B.H. Park, Myeloid sirtuin 6 deficiency accelerates experimental rheumatoid arthritis by enhancing macrophage activation and infiltration into synovium, EBioMedicine 38 (2018) 228–237. https://10.1016/j.ebiom.2018.11.005.

[13] M. Gao, C. Liang, X. Song, Q. Chen, Q. Jin, C. Wang, Z. Liu, Erythrocyte-membrane-enveloped perfluorocarbon as nanoscale artificial red blood cells to relieve tumor hypoxia and enhance cancer radiotherapy, Adv. Mater. 29 (35) (2017). Erythrocyte-Membrane, https://10.1002/adma.201701429.

[14] Z. Duan, Q. Luo, L. Gu, X. Li, H. Zhu, Z. Gu, Q. Gong, H. Zhang, K. Luo, A co-delivery nanoplatform for a lignan-derived compound and perfluorocarbon tuning IL-25 secretion and the oxygen level in tumor microenvironments for meliorative tumor radiotherapy, Nanoscale 13 (32) (2021) 13681–13692. https://10.1039/d1nr03738b.

[15] H. Wang, Y. Guo, C. Wang, X. Jiang, H. Liu, A. Yuan, J. Yan, Y. Hu, J. Wu, Light-controlled oxygen production and collection for sustainable photodynamic therapy in tumor hypoxia, Biomaterials 269 (2021), 120621. https://10.1016/j.biomaterials.2020.120621.

[16] W. Sun, Y. Xu, Y. Yao, J. Yue, Z. Wu, H. Li, G. Shen, Y. Liao, H. Wang, W. Zhou, Self-oxygenation mesoporous MnO(2) nanoparticles with ultra-high drug loading capacity for targeted arteriosclerosis therapy, J. Nanobiotechnol. 20 (1) (2022) 88. https://10.1186/s12951-022-01296-x.

[17] Y. Pu, P. Wang, R. Yang, X. Tan, T. Shi, J. Ma, W. Xue, B. Chi, Bio-fabricated nanocomposite hydrogel with ROS scavenging and local oxygenation accelerates diabetic wound healing, J. Mater. Chem. B 10 (21) (2022) 4083–4095. https://10.1039/d2tb00343k.

[18] Y. Guan, H. Niu, Z. Liu, Y. Dang, J. Shen, M. Zayed, L. Ma, J. Guan, Sustained oxygenation accelerates diabetic wound healing by promoting epithelialization and angiogenesis and decreasing inflammation, Sci. Adv. 7 (35) (2021) eabj0153, https://10.1126/sciadv.abj0153.

[19] Q.X. Chen, J.Y. Li, F. Han, Q.C. Meng, H. Wang, W. Qiang, Z.X. Li, F.F. Li, E. Xie, X.Y. Qin, S. Chen, W.S. Wang, C.Y. Liu, B. Li, F.X. Han, A multifunctional composite hydrogel that rescues the ROS microenvironment and guides the immune response for repair of osteoporotic bone defects, Adv. Funct. Mater. 32 (27) (2022), 2201067, https://10.1002/adfm.202201067.

[20] A. Krinner, M. Zscharnack, A. Bader, D. Drasdo, J. Galle, Impact of oxygen environment on mesenchymal stem cell expansion and chondrogenic differentiation, Cell Prolif 42 (4) (2009) 471–484. https://10.1111/j.1365-2184.2009.00621.x.

[21] A. Napoli, M. Valentini, N. Tirelli, M. Müller, J.A. Hubbell, Oxidation-responsive polymeric vesicles, Nat. Mater. 3 (3) (2004) 183–189. https://10.1038/nmat1081.

[22] T. Wu, X. Chen, Y. Wang, H. Xiao, Y. Peng, L. Lin, W. Xia, M. Long, J. Tao, X. Shuai, Aortic plaque-targeted andrographolide delivery with oxidation-sensitive micelle effectively treats atherosclerosis via simultaneous ROS capture and anti-inflammation, Nanomedicine 14 (7) (2018) 2215–2226. https://10.1016/j.nano.2018.06.010.

[23] P.J. Stiers, N. van Gastel, G. Carmeliet, Targeting the hypoxic response in bone tissue engineering: a balance between supply and consumption to improve bone regeneration, Mol. Cell. Endocrinol. 432 (2016) 96–105. https://10.1016/j.mce.2015.12.024.

[24] J.E. Squires, Artificial blood, Science 295 (5557) (2002) 1002–1005. https://10.1126/science.1068443.

[25] Y. Cheng, H. Cheng, C. Jiang, X. Qiu, K. Wang, W. Huan, A. Yuan, J. Wu, Y. Hu, Perfluorocarbon nanoparticles enhance reactive oxygen levels and tumour growth inhibition in photodynamic therapy, Nat. Commun. 6 (2015) 8785. https://10.1038/ncomms9785.

[26] S. Ramachandran, N.M. Desai, T.A. Goers, N. Benshoff, B. Olack, S. Shenoy, M.D. Jendrisak, W.C. Chapman, T. Mohanakumar, Improved islet yields from pancreas preserved in perflurocarbon is via inhibition of apoptosis mediated by mitochondrial pathway, Am. J. Transplant. 6 (7) (2006) 1696–1703. https://10.1111/j.1600-6143.2006.01368.x.

[27] W. Wang, Y. Cheng, P. Yu, H. Wang, Y. Zhang, H. Xu, Q. Ye, A. Yuan, Y. Hu, J. Wu, Perfluorocarbon regulates the intratumoural environment to enhance hypoxia-based agent efficacy, Nat. Commun. 10 (1) (2019) 1580. https://10.1038/s41467-019-09389-2.

[28] M. Sanchez Dominguez, E. Maillard, M.P. Krafft, S. Sigrist, A. Belcourt, Prevention of adhesion and promotion of pseudoislets formation from a beta-cell line by fluorocarbon emulsions, Chembiochem 7 (8) (2006) 1160–1163. https://10.1002/cbic.200600056.

[29] E. Maillard, M.T. Juszczak, A. Langlois, C. Kleiss, M.C. Sencier, W. Bietiger, M. Sanchez-Dominguez, M.P. Krafft, P.R. Johnson, M. Pinget, S. Sigrist,

Perfluorocarbon emulsions prevent hypoxia of pancreatic β-cells, Cell Transplant. 21 (4) (2012) 657–669. https://10.3727/096368911x593136.

[30] S. Liang, C. Sun, P. Yang, P. Ma, S. Huang, Z. Cheng, X. Yu, J. Lin, Core-shell structured upconversion nanocrystal-dendrimer composite as a carrier for mitochondria targeting and catalase enhanced anti-cancer photodynamic therapy, Biomaterials 240 (2020), 119850. https://10.1016/j.biomaterials.2020.119850.

[31] M. Wen, N. Yu, S. Wu, M. Huang, P. Qiu, Q. Ren, M. Zhu, Z. Chen, On-demand assembly of polymeric nanoparticles for longer-blood-circulation and disassembly in tumor for boosting sonodynamic therapy, Bioact. Mater. 18 (2022) 242–253, https://doi.org/10.1016/j.bioactmat.2022.03.009.

[32] P.K. Chandra, C.L. Ross, L.C. Smith, S.S. Jeong, J. Kim, J.J. Yoo, B.S. Harrison, Peroxide-based oxygen generating topical wound dressing for enhancing healing of dermal wounds, Wound Repair Regen. 23 (6) (2015) 830–841. https://10.1111/wrr.12324.

[33] S. Park, K.M. Park, Hyperbaric oxygen-generating hydrogels, Biomaterials 182 (2018) 234–244. https://10.1016/j.biomaterials.2018.08.032.

[34] F. Dadkhah Tehrani, I. Shabani, A. Shabani, A hybrid oxygen-generating wound dressing based on chitosan thermosensitive hydrogel and decellularized amniotic membrane, Carbohydr. Polym. 281 (2022), 119020, https://10.1016/j.carbpol.2021.119020.

[35] J. Xue, Z. Zhao, L. Zhang, L. Xue, S. Shen, Y. Wen, Z. Wei, L. Wang, L. Kong, H. Sun, Q. Ping, R. Mo, C. Zhang, Neutrophil-mediated anticancer drug delivery for suppression of postoperative malignant glioma recurrence, Nat. Nanotechnol. 12 (7) (2017) 692–700. https://10.1038/nnano.2017.54.

[36] J. Yin, M. Yan, Y. Wang, J. Fu, H. Suo, 3D bioprinting of low-concentration cell-laden gelatin methacrylate (GelMA) bioinks with a two-step cross-linking strategy, ACS Appl. Mater. Interfaces 10 (8) (2018) 6849–6857. https://10.1021/acsami.7b16059.

[37] W. Liu, M.A. Heinrich, Y. Zhou, A. Akpek, N. Hu, X. Liu, X. Guan, Z. Zhong, X. Jin, A. Khademhosseini, Y.S. Zhang, Extrusion bioprinting of shear-thinning gelatin methacryloyl bioinks, Adv Healthc Mater 6 (12) (2017), 1601451. https://10.1002/adhm.201601451.

[38] X.X. Fan, M.Z. Xu, E.L. Leung, C. Jun, Z. Yuan, L. Liu, ROS-responsive berberine polymeric micelles effectively suppressed the inflammation of rheumatoid arthritis by targeting mitochondria, Nano-Micro Lett. 12 (1) (2020) 76. https://10.1007/s40820-020-0410-x.

[39] T. Kamiya, A.H. Kwon, T. Kanemaki, Y. Matsui, S. Uetsuji, T. Okumura, Y. Kamiyama, A simplified model of hypoxic injury in primary cultured rat hepatocytes, in Vitro Cell, Dev Biol Anim 34 (2) (1998) 131–137. https://10.1007/s11626-998-0095-9.

[40] C. Katoh, T. Osanai, H. Tomita, K. Okumura, Brain natriuretic peptide is released from human astrocytoma cell line U373MG under hypoxia: a possible role in anti-apoptosis, J. Endocrinol. 208 (1) (2011) 51–57. https://10.1677/joe-10-0230.

[41] J.M. Brimson, T. Tencomnao, Rhinacanthus nasutus protects cultured neuronal cells against hypoxia induced cell death, Molecules 16 (8) (2011) 6322–6338. https://10.3390/molecules16086322.

[42] H. Cui, S. Wu, Y. Shang, Z. Li, M. Chen, F. Li, C. Wang, Pleurotus nebrodensis polysaccharide(PN50G) evokes A549 cell apoptosis by the ROS/AMPK/PI3K/AKT/mTOR pathway to suppress tumor growth, Food Funct. 7 (3) (2016) 1616–1627. https://10.1039/c6fo00027d.

[43] L. Davies Cde, L.M. Lundstrøm, J. Frengen, L. Eikenes, S.Ø. Bruland, O. Kaalhus, M.H. Hjelstuen, C. Brekken, Radiation improves the distribution and uptake of liposomal doxorubicin (caelyx) in human osteosarcoma xenografts, Cancer Res. 64 (2) (2004) 547–553. https://10.1158/0008-5472.can-03-0576.

[44] Z. Khan, G.K. Michalopoulos, D.B. Stolz, Peroxisomal localization of hypoxia-inducible factors and hypoxia-inducible factor regulatory hydroxylases in primary rat hepatocytes exposed to hypoxia-reoxygenation, Am. J. Pathol. 169 (4) (2006) 1251–1269. https://10.2353/ajpath.2006.060360.

[45] X. Zhang, Y. Xu, X. Xu, J. Zhu, L. Chen, Y. Xu, Y. Yang, N. Song, Bevacizumab-laden nanofibers simulating an antiangiogenic niche to improve the submuscular stability of stem cell engineered cartilage, Small 18 (23) (2022), e2201874. https://10.1002/smll.202201874.

[46] S. Lee, T.Y. Lee, E. Amstad, S.H. Kim, Microfluidic production of capsules-in-capsules for programed release of multiple ingredients, Advanced Materials Technologies 3 (5) (2018), 1800006. https://10.1002/admt.201800006.

[47] A. Nandi, L.J. Yan, C.K. Jana, N. Das, Role of catalase in oxidative stress- and age-associated degenerative diseases, Oxid. Med. Cell. Longev. (2019), 9613090, 2019, https://10.1155/2019/9613090.

[48] J.F. Turrens, J.D. Crapo, B.A. Freeman, Protection against oxygen toxicity by intravenous injection of liposome-entrapped catalase and superoxide dismutase, J. Clin. Invest. 73 (1) (1984) 87–95. https://10.1172/jci111210.

[49] R. Zhang, X. Song, C. Liang, X. Yi, G. Song, Y. Zhao, Y. Yang, K. Yang, L. Feng, Z. Liu, Catalase-loaded cisplatin-prodrug-constructed liposomes to overcome tumor hypoxia for enhanced chemo-radiotherapy of cancer, Biomaterials 138 (2017) 13–21. https://10.1016/j.biomaterials.2017.05.025.

[50] S. Shah, V. Dhawan, R. Holm, M. Nagarsenker, Y. Perrie, Liposomes: advancements and innovation in the manufacturing process, Adv. Drug Deliv. Rev. (2020) 102–122. https://10.1016/j.addr.2020.07.002.

[51] K. Yue, G. Trujillo-de Santiago, M.M. Alvarez, A. Tamayol, N. Annabi, A. Khademhosseini, Synthesis, properties, and biomedical applications of gelatin methacryloyl (GelMA) hydrogels, Biomaterials 73 (2015) 254–271. https://10.1016/j.biomaterials.2015.08.045.

[52] Z. Li, S. Xiang, Z. Lin, E.N. Li, H. Yagi, G. Cao, L. Yocum, L. Li, T. Hao, K.K. Bruce, M.R. Fritch, H. Hu, B. Wang, P.G. Alexander, K.A. Khor, R.S. Tuan, H. Lin, Graphene oxide-functionalized nanocomposites promote osteogenesis of human

[53] mesenchymal stem cells via enhancement of BMP-SMAD1/5 signaling pathway, Biomaterials 277 (2021), 121082. https://10.1016/j.biomaterials.2021.121082.

[53] K.L. Spiller, S.A. Maher, A.M. Lowman, Hydrogels for the repair of articular cartilage defects, Tissue Eng. B Rev. 17 (4) (2011) 281–299. https://10.1089/ten.TEB.2011.0077.

[54] H.T. Nguyen, M. Ono, Y. Oida, E.S. Hara, T. Komori, K. Akiyama, H.T.T. Nguyen, K.T. Aung, H.T. Pham, I. Tosa, T. Takarada, K. Matsuo, T. Mizoguchi, T. Oohashi, T. Kuboki, Bone marrow cells inhibit BMP-2-induced osteoblast activity in the marrow environment, J. Bone Miner. Res. 34 (2) (2019) 327–332. https://10.1002/jbmr.3598.

[55] K.L. Spiller, Y. Liu, J.L. Holloway, S.A. Maher, Y. Cao, W. Liu, G. Zhou, A.M. Lowman, A novel method for the direct fabrication of growth factor-loaded microspheres within porous nondegradable hydrogels: controlled release for cartilage tissue engineering, J. Contr. Release 157 (1) (2012) 39–45. https://10.1016/j.conrel.2011.09.057.

[56] A.H. Nguyen, J. McKinney, T. Miller, T. Bongiorno, T.C. McDevitt, Gelatin methacrylate microspheres for controlled growth factor release, Acta Biomater. 13 (2015) 101–110. https://10.1016/j.actbio.2014.11.028.

[57] N. Koike, D. Fukumura, O. Gralla, P. Au, J.S. Schechner, R.K. Jain, Tissue engineering: creation of long-lasting blood vessels, Nature 428 (6979) (2004) 138–139. https://10.1038/428138a.

[58] S. Das, S. Singh, J.M. Dowding, S. Oommen, A. Kumar, T.X. Sayle, S. Saraf, C.R. Patra, N.E. Vlahakis, D.C. Sayle, W.T. Self, S. Seal, The induction of angiogenesis by cerium oxide nanoparticles through the modulation of oxygen in intracellular environments, Biomaterials 33 (31) (2012) 7746–7755. https://10.1016/j.biomaterials.2012.07.019.

[59] Y. Guan, N. Gao, H. Niu, Y. Dang, J. Guan, Oxygen-release microspheres capable of releasing oxygen in response to environmental oxygen level to improve stem cell survival and tissue regeneration in ischemic hindlimbs, J. Contr. Release 331 (2021) 376–389. https://10.1016/j.jconrel.2021.01.034.

[60] R.T. Mendes, D. Nguyen, D. Stephens, F. Pamuk, D. Fernandes, H. Hasturk, T.E. Van Dyke, A. Kantarci, Hypoxia-induced endothelial cell responses - possible roles during periodontal disease, Clin Exp Dent Res 4 (6) (2018) 241–248. https://10.1002/cre2.135.

[61] H.M. Wong, Y.Y. Zhang, Q.L. Li, An enamel-inspired bioactive material with multiscale structure and antibacterial adhesion property, Bioact. Mater. 7 (2022) 491–503. https://10.1016/j.bioactmat.2021.05.035.

[62] S.S. Hannah, S. McFadden, A. McNeilly, C. McClean, Take my bone away?" hypoxia and bone: a narrative review, J. Cell. Physiol. 236 (2) (2021) 721–740. https://10.1002/jcp.29921.

[63] J.C. Utting, S.P. Robins, A. Brandao-Burch, I.R. Orriss, J. Behar, T.R. Arnett, Hypoxia inhibits the growth, differentiation and bone-forming capacity of rat osteoblasts, Exp. Cell Res. 312 (10) (2006) 1693–1702. https://10.1016/j.yexcr.2006.02.007.

[64] W.K. Kim, V. Meliton, N. Bourquard, T.J. Hahn, F. Parhami, Hedgehog signaling and osteogenic differentiation in multipotent bone marrow stromal cells are inhibited by oxidative stress, J. Cell. Biochem. 111 (5) (2010) 1199–1209. https://10.1002/jcb.22846.

[65] A. Salim, R.P. Nacamuli, E.F. Morgan, A.J. Giaccia, M.T. Longaker, Transient changes in oxygen tension inhibit osteogenic differentiation and Runx2 expression in osteoblasts, J. Biol. Chem. 279 (38) (2004) 40007–40016. https://10.1074/jbc.M403715200.

[66] M.H. Sun, W.J. Wang, Q. Li, T. Yuan, W.J. Weng, Autologous oxygen release nano bionic scaffold composite miR-106a induced BMSCs enhances osteoblast conversion and promotes bone repair through regulating BMP-2, Eur. Rev. Med. Pharmacol. Sci. 22 (21) (2018) 7148–7155. https://10.26355/eurrev_201811_16246.

[67] H. Enomoto, T. Furuichi, A. Zanma, K. Yamana, C. Yoshida, S. Sumitani, H. Yamamoto, M. Enomoto-Iwamoto, M. Iwamoto, T. Komori, Runx2 deficiency in chondrocytes causes adipogenic changes in vitro, J. Cell Sci. 117 (Pt 3) (2004) 417–425. https://10.1242/jcs.00866.

[68] A. Forlino, W.A. Cabral, A.M. Barnes, J.C. Marini, New perspectives on osteogenesis imperfecta, Nat. Rev. Endocrinol. 7 (9) (2011) 540–557. https://10.1038/nrendo.2011.81.

[69] K.T. Sun, M.Y. Chen, M.G. Tu, I.K. Wang, S.S. Chang, C.Y. Li, MicroRNA-20a regulates autophagy related protein-ATG16L1 in hypoxia-induced osteoclast differentiation, Bone 73 (2015) 145–153. https://10.1016/j.bone.2014.11.026.

[70] K. Murata, C. Fang, C. Terao, E.G. Giannopoulou, Y.J. Lee, M.J. Lee, S.H. Mun, S. Bae, Y. Qiao, R. Yuan, M. Furu, H. Ito, K. Ohmura, S. Matsuda, T. Mimori, F. Matsuda, K.H. Park-Min, L.B. Ivashkiv, Hypoxia-Sensitive COMMD1 integrates signaling and cellular metabolism in human macrophages and suppresses osteoclastogenesis, Immunity 47 (1) (2017) 66–79, e65, https://10.1016/j.immuni.2017.06.018.

[71] Y. Tang, J. Zhu, D. Huang, X. Hu, Y. Cai, X. Song, Z. Song, C. Hong, Z. Feng, F. Kang, Mandibular osteotomy-induced hypoxia enhances osteoclast activation and acid secretion by increasing glycolysis, J. Cell. Physiol. 234 (7) (2019) 11165–11175. https://10.1002/jcp.27765.

[72] Y. Zhao, G. Chen, W. Zhang, N. Xu, J.Y. Zhu, J. Jia, Z.J. Sun, Y.N. Wang, Y.F. Zhao, Autophagy regulates hypoxia-induced osteoclastogenesis through the HIF-1α/BNIP3 signaling pathway, J. Cell. Physiol. 227 (2) (2012) 639–648.

[73] I. Rabinovich-Nikitin, M. Rasouli, C.J. Reitz, I. Posen, V. Margulets, R. Dhingra, T.N. Khatua, J.A. Thliveris, T.A. Martino, L.A. Kirshenbaum, Mitochondrial autophagy and cell survival is regulated by the circadian Clock gene in cardiac myocytes during ischemic stress, Autophagy 17 (11) (2021) 3794–3812. https://10.1080/15548627.2021.1938913.

[74] Z. Qian, Y. Zhang, X. Kang, H. Li, Y. Zhang, X. Jin, X. Gao, M. Xu, Z. Ma, L. Zhao, Z. Zhang, H. Sun, S. Wu, Postnatal conditional deletion of Bmal1 in osteoblasts enhances trabecular bone formation via increased BMP2 signals, J. Bone Miner. Res. 35 (8) (2020) 1481–1493. https://10.1002/jbmr.4017.

[75] A. Stangherlin, A.B. Reddy, Regulation of circadian clocks by redox homeostasis, J. Biol. Chem. 288 (37) (2013) 26505–26511. https://10.1074/jbc.R113.457564.

[76] R.V. Kondratov, O. Vykhovanets, A.A. Kondratova, M.P. Antoch, Antioxidant N-acetyl-L-cysteine ameliorates symptoms of premature aging associated with the deficiency of the circadian protein BMAL1, Aging (Albany NY) 1 (12) (2009) 979–987. https://10.18632/aging.100113.

[77] T. Finkel, Signal transduction by reactive oxygen species, J. Cell Biol. 194 (1) (2011) 7–15. https://10.1083/jcb.201102095.

[78] L. Liu, Q. Cao, W. Gao, B.Y. Li, B. Zeng, Z. Xia, B. Zhao, Melatonin ameliorates cerebral ischemia-reperfusion injury in diabetic mice by enhancing autophagy via the SIRT1-BMAL1 pathway, Faseb. J. 35 (12) (2021), e22040. https://10.1096/fj.202002718RR.

[79] O. Al-Sawaf, T. Clarner, A. Fragoulis, Y.W. Kan, T. Pufe, K. Streetz, C.J. Wruck, Nrf2 in health and disease: current and future clinical implications, Clin Sci (Lond). 129 (12) (2015) 989–999. https://10.1042/cs20150436.

[80] T.S. Gross, K.A. King, N.A. Rabaia, P. Pathare, S. Srinivasan, Upregulation of osteopontin by osteocytes deprived of mechanical loading or oxygen, J. Bone Miner. Res. 20 (2) (2005) 250–256. https://10.1359/jbmr.041004.

[81] T.R. Arnett, Acidosis, hypoxia and bone, Arch. Biochem. Biophys. 503 (1) (2010) 103–109. https://10.1016/j.abb.2010.07.021.

[82] R. Tevlin, E.Y. Seo, O. Marecic, A. McArdle, X. Tong, B. Zimdahl, A. Malkovskiy, R. Sinha, G. Gulati, X. Li, T. Wearda, R. Morganti, M. Lopez, R.C. Ransom, C. R. Duldulao, M. Rodrigues, A. Nguyen, M. Januszyk, Z. Maan, K. Paik, K.S. Yapa, J. Rajadas, D.C. Wan, G.C. Gurtner, M. Snyder, P.A. Beachy, F. Yang, S. B. Goodman, I.L. Weissman, C.K. Chan, M.T. Longaker, Pharmacological rescue of diabetic skeletal stem cell niches, Sci. Transl. Med. 9 (372) (2017), eaag2809. https://10.1126/scitranslmed.aag2809.

[83] S. Heltmann-Meyer, D. Steiner, C. Müller, D. Schneidereit, O. Friedrich, S. Salehi, F.B. Engel, A. Arkudas, R.E. Horch, Gelatin methacryloyl is a slow degrading material allowing vascularization and long-term use in vivo, Biomed. Mater. 16 (6) (2021). https://10.1088/1748-605X/ac1e9d.

[84] Y. Wang, C. Xie, Z. Zhang, H. Liu, H. Xu, Z. Peng, C. Liu, J. Li, C. Wang, T. Xu, L. Zhu, 3D printed integrated bionic oxygenated scaffold for bone regeneration, ACS Appl. Mater. Interfaces 14 (26) (2022) 29506–29520. https://10.1021/acsami.2c04378.

[85] M. von Otter, S. Landgren, S. Nilsson, M. Zetterberg, D. Celojevic, P. Bergström, L. Minthon, N. Bogdanovic, N. Andreasen, D.R. Gustafson, I. Skoog, A. Wallin, G. Tasa, K. Blennow, M. Nilsson, O. Hammarsten, H. Zetterberg, Nrf2-encoding NFE2L2 haplotypes influence disease progression but not risk in Alzheimer's disease and age-related cataract, Mech. Ageing Dev. 131 (2) (2010) 105–110. https://10.1016/j.mad.2009.12.007.

[86] J. Xu, T. Chu, T. Yu, N. Li, C. Wang, C. Li, Y. Zhang, H. Meng, G. Nie, Design of diselenide-bridged hyaluronic acid nano-antioxidant for efficient ROS scavenging to relieve colitis, ACS Nano (2022) 13037–13048. https://10.1021/acsnano.2c05558.

[87] Y. Sun, H. Xu, B. Tan, Q. Yi, H. Liu, T. Chen, H. Xiang, R. Wang, Q. Xie, J. Tian, J. Zhu, Andrographolide protects bone marrow mesenchymal stem cells against glucose and serum deprivation under hypoxia via the NRF2 signaling pathway, Stem Cell Res. Ther. 13 (1) (2022) 326. https://10.1186/s13287-022-03016-6.

[88] F. Long, Building strong bones: molecular regulation of the osteoblast lineage, Nat. Rev. Mol. Cell Biol. 13 (1) (2011) 27–38. https://10.1038/nrm3254.

[89] H.H. Xu, P. Wang, L. Wang, C. Bao, Q. Chen, M.D. Weir, L.C. Chow, L. Zhao, X. Zhou, M.A. Reynolds, Calcium phosphate cements for bone engineering and

[90] C. Shuai, W. Yang, P. Feng, S. Peng, H. Pan, Accelerated degradation of HAP/PLLA bone scaffold by PGA blending facilitates bioactivity and osteoconductivity, Bioact. Mater. 6 (2) (2021) 490–502. https://10.1016/j.bioactmat.2020.09.001.

[91] G. Caligiuri, CD31 as a therapeutic target in atherosclerosis, Circ. Res. 126 (9) (2020) 1178–1189. https://10.1161/circresaha.120.315935.

[92] F. Shalaby, J. Rossant, T.P. Yamaguchi, M. Gertsenstein, X.F. Wu, M.L. Breitman, A.C. Schuh, Failure of blood-island formation and vasculogenesis in Flk-1-deficient mice, Nature 376 (6535) (1995) 62–66. https://10.1038/376062a0.

[93] A. Niethammer, R. Xiang, J. Becker, H. Wodrich, U. Pertl, G. Karsten, B. Eliceiri, R. Reisfeld, A DNA vaccine against VEGF receptor 2 prevents effective angiogenesis and inhibits tumor growth, Nat. Med. 8 (12) (2002) 1369–1375. https://10.1038/nm1202-794.

[94] H.W. Hopf, J.J. Gibson, A.P. Angeles, J.S. Constant, J.J. Feng, M.D. Rollins, M. Zamirul Hussain, T.K. Hunt, Hyperoxia and angiogenesis, Wound Repair Regen. 13 (6) (2005) 558–564. https://10.1111/j.1524-475X.2005.00078.x.

[95] A. Farzin, S. Hassan, L.S.M. Teixeira, M. Gurian, J.F. Crispim, V. Manhas, A. Carlier, H. Bae, L. Geris, I. Noshadi, S.R. Shin, J. Leijten, Self-oxygenation of tissues orchestrates full-thickness vascularization of living implants, Adv. Funct. Mater. 31 (42) (2021), 2100850, https://10.1002/adfm.202100850.

[96] J.R. Soucy, E. Shirzaei Sani, R. Portillo Lara, D. Diaz, F. Dias, A.S. Weiss, A. N. Koppes, R.A. Koppes, N. Annabi, Photocrosslinkable gelatin/tropoelastin hydrogel adhesives for peripheral nerve repair, Tissue Eng. 24 (17–18) (2018) 1393–1405. https://10.1089/ten.TEA.2017.0502.

[97] Y. Sun, X. Yao, Q.J. Zhang, M. Zhu, Z.P. Liu, B. Ci, Y. Xie, D. Carlson, B. A. Rothermel, Y. Sun, B. Levine, J.A. Hill, S.E. Wolf, J.P. Minei, Q.S. Zang, Beclin-1-Dependent autophagy protects the heart during sepsis, Circulation 138 (20) (2018) 2247–2262. https://10.1161/circulationaha.117.032821.

[98] C. Maes, G. Carmeliet, E. Schipani, Hypoxia-driven pathways in bone development, regeneration and disease, Nat. Rev. Rheumatol. 8 (6) (2012) 358–366. https://10.1038/nrrheum.2012.36.

[99] C.B. Peek, D.C. Levine, J. Cedernaes, A. Taguchi, Y. Kobayashi, S.J. Tsai, N. A. Bonar, M.R. McNulty, K.M. Ramsey, J. Bass, Circadian clock interaction with HIF1α mediates oxygenic metabolism and anaerobic glycolysis in skeletal muscle, Cell Metabol. 25 (1) (2017) 86–92. https://10.1016/j.cmet.2016.09.010.

[100] Y. Wu, D. Tang, N. Liu, W. Xiong, H. Huang, Y. Li, Z. Ma, H. Zhao, P. Chen, X. Qi, E.E. Zhang, Reciprocal regulation between the circadian clock and hypoxia signaling at the genome level in mammals, Cell Metabol. 25 (1) (2017) 73–85. https://10.1016/j.cmet.2016.09.009.

[101] B. Xu, P.B. Zheng, F. Gao, W. Wang, H.T. Zhang, X.R. Zhang, X.Q. Feng, W.G. Liu, A mineralized high strength and tough hydrogel for skull bone regeneration, Adv. Funct. Mater. 27 (4) (2017), 1604327. https://10.1002/adfm.201604327.

[102] S. Shanbhag, C. Kampleitner, S. Mohamed-Ahmed, M.A. Yassin, H. Dongre, D. E. Costea, S. Tangl, A. Stavropoulos, A.I. Bolstad, S. Suliman, K. Mustafa, Ectopic bone tissue engineering in mice using human gingiva or bone marrow-derived stromal/progenitor cells in scaffold-hydrogel constructs, Front. Bioeng. Biotechnol. 9 (2021), 783468. https://10.3389/fbioe.2021.783468.

[103] J. Li, W. Wang, M. Li, P. Song, H. Lei, X. Gui, C. Zhou, L. Liu, Biomimetic methacrylated gelatin hydrogel loaded with bone marrow mesenchymal stem cells for bone tissue regeneration, Front. Bioeng. Biotechnol. 9 (2021), 770049. https://10.3389/fbioe.2021.770049.

[104] M.F. Pittenger, D.E. Discher, B.M. Péault, D.G. Phinney, J.M. Hare, A.I. Caplan, Mesenchymal stem cell perspective: cell biology to clinical progress, NPJ Regen Med 4 (2019) 22. https://10.1038/s41536-019-0083-6.